RPT-2017-049, Revision 0

GEOPHYSICAL CHARACTERIZATION OF THE PEG LEG SITE, RESOLUTION MINE, AZ

C. Baldyga
G. Noonan
J. Strohmeyer
B. Cubbage

hydroGEOPHYSICS

2302 N. Forbes Blvd, Tucson, AZ 85745 USA

Date Published
November 2017

Prepared for Resolution Copper Mine

Executive Summary

In September of 2017, HGI conducted a multi-method electrical resistivity, refraction seismic, and gravity geophysical survey at a proposed Tailings Storage Facility (TSF) called the Peg Leg TSF, near Kearny, Arizona. The survey was designed to help answer questions about the depths to bedrock and character of the basin fill in support of a geotechnical feasibility study for the proposed TSF.

Prior to the survey there were no deep boreholes within the basin itself to help shape the geophysical survey design so the original specifications of these surveys was to image down to a bedrock interface which was presumed to be 250ft bgs. The seismic data collection began on Line 1 and within a few hours of initial data collection it was observed that the data indicated that we were only seeing basin fill materials down to an approximate imaging depth of 300 ft bgs before it exceeded the limitations of the seismic refraction equipment being used. The initial electrical resistivity data that were collected on the first day also showed that we were only imaging basin fill with no indication of bedrock conditions but to a deeper imaging limitation depth of 400ft bgs. At that point the survey design was revamped by reducing the scope of the electrical and seismic surveying to a few select lines, and including a basin wide gravity survey, which was the next logical step to image down to the deeper-than-expected bedrock.

Figure ES-1 shows the combined results of Line 1 where the three methods augment each other very well. Line 1 was shifted from its initial placement to a new location where exposed bedrock was present; data were collected starting on the eastern edge of the outcrop and headed westwards where bedrock was believed to deepen. Moving the survey westward in this manner allowed HGI to observe the slope of the bedrock interface until it was too deep to image with the electrical or seismic imaging techniques.

Figure ES- 1. Line 1 Combined Geophysical Results.

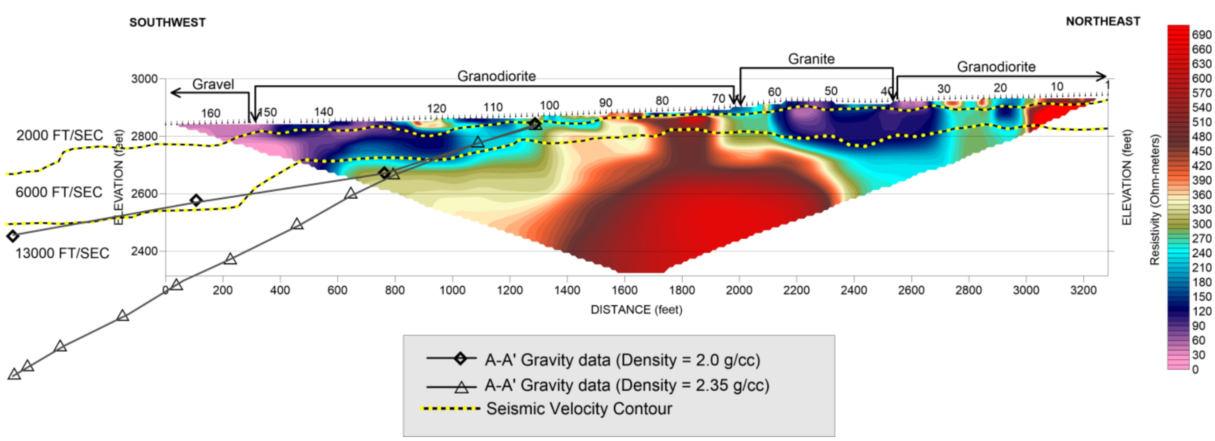

TABLE OF CONTENTS

LIST OF FIGURES

LIST OF TABLES

1.0 INTRODUCTION

1.1 PROJECT DESCRIPTION

In September 2017, hydroGEOPHYSICS, Inc. (HGI), under contract to Resolution Copper Mining Ltd (RCML), performed a geophysical survey to investigate shallow groundwater conditions, quaternary deposits, and bedrock at a proposed Tailings Storage Facility (TSF) called the Peg Leg TSF, near Kearny, AZ. The purpose of the shallow geophysical survey was to provide greater understanding of subsurface conditions.

1.2 SITE LOCATION

The Peg Leg Site is located in central Arizona within Pinal County, approximately 10 miles west of Kearny, Arizona. Figure 1 shows the general location of the geophysical survey.

1.3 OBJECTIVE OF INVESTIGATION

The objective of the overall geophysical survey was to image depths to bedrock and evaluate changes in alluvial fill in support of a larger program looking at the geotechnical feasibility of the proposed Peg Leg TSF. The geophysical survey, as proposed, was designed to:

- Assess thickness and variability of Quaternary deposits within the potential TSF footprint,
- Map the depth to phreatic surface within the potential TSF footprint,
- Assess thickness and variability of Quaternary deposits downstream of potential TSF footprint,
- Assess depth to phreatic surface downstream of potential TSF footprint.

1.4 SCOPE OF INVESTIGATION

Three geophysical methods were employed and co-analyzed to characterize the site: Electrical Resistivity, Refraction P-wave Seismics, and Gravity. The geophysical program was initially designed to solely use the seismic refraction and electrical resistivity methods to define depths to bedrock and characterize alluvial fill above bedrock along pre-defined areas of interest to Resolution. The conceptual model going into the project was that bedrock may be as shallow as 250 feet, and as such, the seismic survey was designed to image down to about 300 feet below ground surface (bgs) which is about the limitation of the seismic refraction method. The electrical resistivity survey was designed to image down to a maximum depth of 600 feet bgs.

On the first day of the geophysical program, HGI began seismic data collection on Line 2 and electrical resistivity data collection on Line 3 (about a half mile to the west of Line 2). Data were immediately evaluated during that first field day and the seismic data indicated that only alluvium was being encountered, with no indication of bedrock. Simultaneously, the electrical resistivity data were evaluated in the field and indicated the same interpretation - that only alluvial fill was being imaged. At this point, the seismic and resistivity surveys were re-designed to answer different questions, and a gravity survey was then designed to image depth to bedrock in the deeper parts of the basin.

Electrical resistivity was used to measure electrical properties of the subsurface, which are greatly influenced by the moisture content (phreatic surface) and grain size distribution (clays vs gravels). Electrical resistivity may also be used to help validate bedrock topography if there are strong contrasts between the overlying sediments and underlying rock. Three electrical resistivity lines were collected, ranging from 918 to 1002 meters (~3012 to 3287 feet) in length. The electrical resistivity data were processed and are presented as inverse modeled two-dimensional (2D) profiles.

P-Wave seismic refraction was used for determining depth to bedrock and bedrock structure. Seismic data were collected along two transects, both in conjunction with resistivity line locations. The seismic data were modeled and results were combined with resistivity results as plot overlays of layer velocity.

Three gravity models were prepared for this study that provide depth to bedrock estimations within the area, which took into account some of the information obtained by the drilling campaign conducted by Resolution Copper in the Far West site in 2012. This site is located 4 miles east of Florence Junction in Pinal County, AZ. The purpose of the 2010 Far West project was to define the depth to bedrock for proposed drilling locations that we later drilled in 2012.

Figure 1. General Location Map.

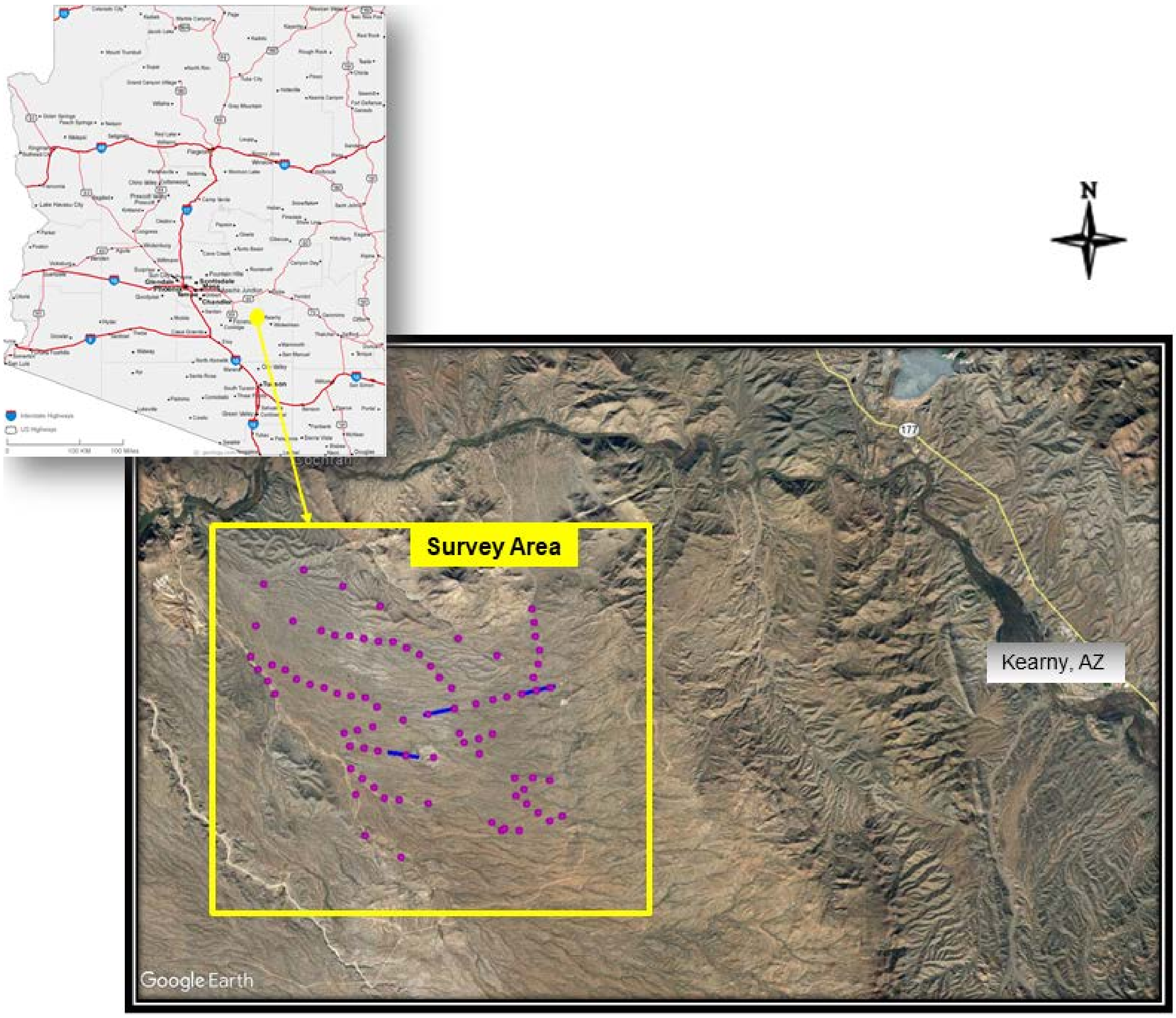

Imagery Source 2017 Google Earth

2.0 GEOPHYSICAL THEORY

2.1 ELECTRICAL RESISTIVITY

Electrical resistivity is a volumetric property that describes the resistance of electrical current flow within a medium (Rucker et al., 2011; Telford et al., 1990). Direct electrical current is propagated in rocks and minerals by electronic or electrolytic means. Electronic conduction occurs in minerals where free electrons are available, such as the electrical current flow through metal. Electrolytic conduction, on the other hand, relies on the dissociation of ionic species within a pore space. With electrolytic conduction, the movement of electrons varies with the mobility, concentration, and the degree of dissociation of the ions.

Mechanistically, the resistivity method uses electric current (I) that is transmitted into the earth through one pair of electrodes (transmitting dipole) that are in contact with the soil. The resultant voltage potential (V) is then measured across another pair of electrodes (receiving dipole). Numerous electrodes can be deployed along a transect (which may be anywhere from feet to miles in length), or within a grid. Figure 2 shows examples of electrode layouts for surveying. The figure shows transects with a variety of array types (dipole-dipole, Schlumberger, pole-pole). A complete set of measurements occurs when each electrode (or adjacent electrode pair) passes current, while all other adjacent electrode pairs are utilized for voltage measurements. Modern equipment automatically switches the transmitting and receiving electrode pairs through a single multi-core cable connection. Rucker et al. (2009) describe in more detail the methodology for efficiently conducting an electrical resistivity survey.

Figure 2. Possible Arrays for Use in Electrical Resistivity Characterization

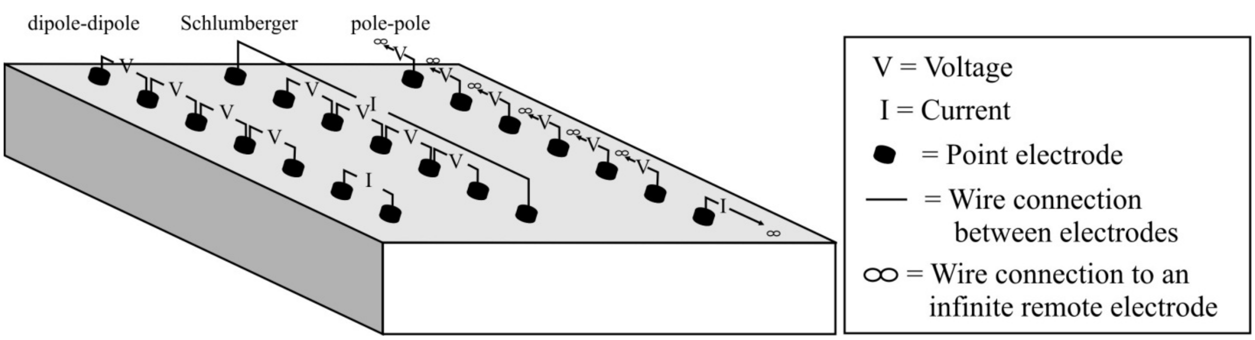

The modern application of the resistivity method uses numerical modeling and inversion theory to estimate the electrical resistivity distribution of the subsurface given the known quantities of electrical current, measured voltage, and electrode positions. A common resistivity inverse method incorporated in commercially available codes is the regularized least squares optimization method (Sasaki, 1989; Loke, et al., 2003). The objective function within the optimization aims to minimize the difference between measured and modeled potentials (subject to certain constraints, such as the type and degree of spatial smoothing or regularization) and the optimization is conducted iteratively due to the nonlinear nature of the model that describes the potential distribution. The relationship between the subsurface resistivity (ρ) and the measured voltage is given by the following equation (from Dey and Morrison, 1979):

$$-\nabla \cdot \left[\frac{1}{\rho(x,y,z)} \nabla V(x,y,z) \right] = \left(\frac{I}{U} \right) \delta(x - x_s)\delta(y - y_s)\delta(z - z_s) \qquad (1)$$

where I is the current applied over an elemental volume U specified at a point (x_s, y_s, z_s) by the Dirac delta function.

Equation (1) is solved many times over the volume of the earth by iteratively updating the resistivity model values using either the L_2-norm smoothness-constrained least squares method, which aims to minimize the square of the misfit between the measured and modeled data (de Groot-Hedlin & Constable, 1990; Ellis & Oldenburg, 1994):

$$\left(J_i^T J_i + \lambda_i W^T W \right) \Delta r_i = J_i^T g_i - \lambda_i W^T W r_{i-1} \qquad (2)$$

or the L_1-norm that minimizes the sum of the absolute value of the misfit:

$$\left(J_i^T R_d J_i + \lambda_i W^T R_m W \right) \Delta r_i = J_i^T R_d g_i - \lambda_i W^T R_m W r_{i-1} \qquad (1)$$

where g is the data misfit vector containing the difference between the measured and modeled data, J is the Jacobian matrix of partial derivatives, W is a roughness filter, R_d and R_m are the weighting matrices to equate model misfit and model roughness, Δr_i is the change in model parameters for the i^{th} iteration, r_i is the model parameters for the previous iteration, and λ_i = the damping factor.

2.2 P-WAVE SEISMIC REFRACTION

The P-wave seismic refraction method is based on the measurement of the travel time of seismic compressional waves refracted at the interfaces between subsurface layers of different velocity. Figure 3 shows an example of the seismic refraction method. Seismic energy is provided by a source ('shot') located on the surface. For shallow applications, the shot normally comprises a hammer and plate, weight drop, or small explosive charge (blank shotgun cartridge). Energy radiates out from the shot point, either traveling directly through the upper layer (direct arrivals), or traveling down to and then laterally along higher velocity layers (refracted arrivals) before returning to the surface. The refracted energy is detected on the surface using a linear array (or spread) of geophones spaced at regular intervals. Beyond a certain distance from the shot point, known as the cross-over distance, the refracted signal is observed as a first-arrival signal at the geophones (arriving before the direct arrival). Observation of the travel times of the direct and refracted signals provides information on the depth profile of the refractor.

Figure 3. Ray Travel for Seismic Refraction Surveying

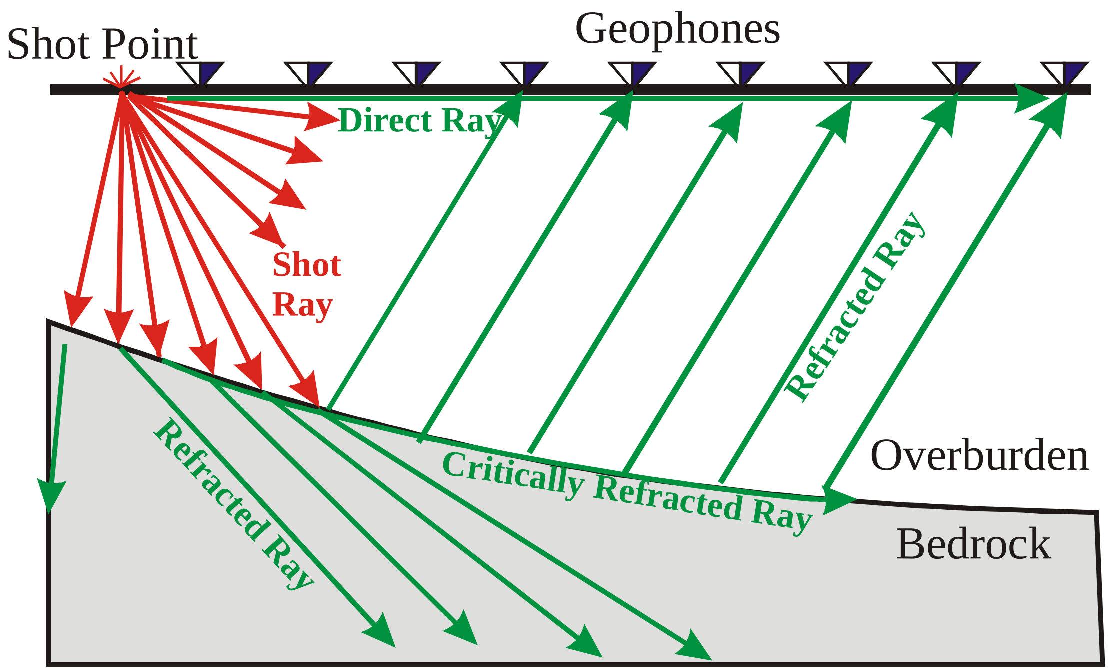

Data are recorded on a seismograph and later downloaded to a computer for analysis of the first-arrival times to the geophones from each shot position. Travel-time versus distance graphs are then constructed and velocities calculated for the overburden and refractor layers through analysis of the direct arrival and T-minus graph gradients. Depth profiles for each refractor are produced by an analytical procedure based on consideration of shot and receiver geometry and the measured travel-times and calculated velocities. The final output comprises a depth profile of the refractor layer and a velocity model of the subsurface.

The primary applications of seismic refraction are for determining depth to bedrock and bedrock structure. Due to the dependence of seismic velocity on the elasticity and density of the material through which the energy is passing, seismic refraction surveys provide a measure of material strengths and can consequently be used as an aid in assessing rippability and rock quality. The technique has been successfully applied to mapping depth to base of backfilled quarries, depth of landfills, thickness of overburden, voids, and the topography of groundwater.

2.3 GRAVITY

Gravity is measured as acceleration due to gravitational pull, or gravitational force per unit mass. Measurements of gravity are presented in units of milligals (abbreviated mgal), which are 10-3

Gal (1 Gal = 1 centimeter per second per second equals 10-2 meters per second per second equals 10-2 newton per kilogram). The Earth's nominal gravity is 980 Gal.

Gravity surveying is a geophysical method that aids in determining the depth to bedrock, overall basin geometry within and surrounding a site, and relative lateral changes in bedrock densities. Lateral differences in gravitational attraction are caused by contrasting densities of geologic media, such as alluvium versus bedrock, along with other external influences; these external influences are accounted for in numerical processing after data acquisition is complete. The information gained from the survey determines relative changes in bedrock character over a defined investigation area. Gravity surveying can also define the locations of fault zones provided there is a lateral change in density across the fault escarpment. Generally speaking, inflection points in gravity profiles are usually located directly above the fault and for the case of a buried ore deposit or volcanic flow, the inflection points are located above the edges of body. Qualitatively speaking, a sharp high frequency anomaly is indicative of a shallow body causing the anomaly versus a low frequency anomaly, which is a good indication of a deeply buried body. Due to the overlapping range in densities of alluvium the gravity method is not the leading method for detecting different thicknesses of sedimentary formations i.e. sands versus clay units.

By acquiring numerous gravity measurements within a study area at discrete points, a contoured gravitational map is developed. The map is used to determine the location of thick, lower density alluvial deposits versus higher density and shallow bedrock. Acquired field data are processed and typically presented in both plan and modeled cross-sectional plots.

In many areas that are "exploratory" in nature, geologic data, and in particular density data, are insufficient to conduct well-constrained forward modeling and results in a "non-unique" solution. In other words, several plausible geologic models can be constructed to fit the observed gravity data.

3.0 METHODOLOGY

3.1 SURVEY AREA AND LOGISTICS

The multi-method geophysical survey was conducted between September 7th and 17th, 2017. Figure 4 shows an overview of the coverage for the three geophysical methods performed, along with the outline of the potential boundary for the tailings storage facility (TSF), as provided by the client.

Figure 4. Site Map with Geophysical Survey Lines and Station Locations.

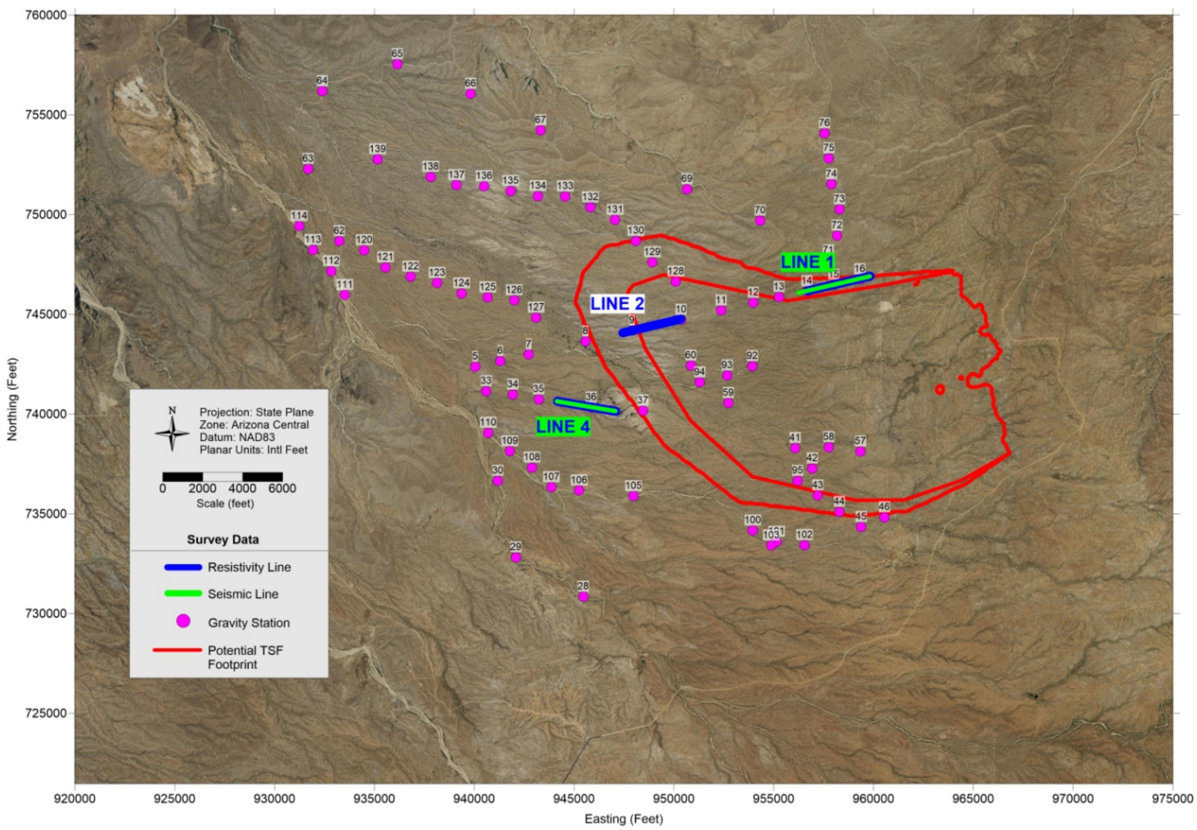

3.1.1 Resistivity Data Acquisition

Three lines of resistivity data were acquired with survey parameters as detailed in Table 1. Geophysical cables with 6-meter spaced stainless steel electrodes were used along with a Wenner array for acquisition of the electrical resistivity data. Additional resistivity lines were originally proposed (seven lines total); however, preliminary analysis of data as it was acquired showed that the bedrock was deeper than the imaging depth of the method and the proposed survey design was modified to include only three of the originally proposed lines. The line names/numbers retained and acquired of the original proposed lines are Lines 1, 2, and 4.

Table 1. Resistivity Survey Details

Line Name	Date(s) of Acquisition	Direction of Collection	Electrode Spacing	Line Length
Line 1	9/10/2017, 9/11/2017	East to West	6m (~20ft)	1002m (~3287ft)
Line 2	9/7/2017	West to East	6m (~20ft)	918m (~3012ft)
Line 4	9/9/2017	West to East	6m (~20ft)	918m (~3012ft)

3.1.2 Seismic Data Acquisition

Two lines of seismic P-wave refraction data were acquired with survey parameters as detailed in Table 2. The seismic lines were co-located with two of the resistivity lines, Lines 1 and 4 to allow for combined method analysis. 14Hz geophone placement was every 20 feet, shot point spacing was 60-feet located at the midpoint of geophone positions along the spread, with off-end shots at 50 and 144 feet beyond the first and last geophones. The seismic source consisted of a hitch mounted elastic wave generator with a 40 kilogram weight drop (PEG-40). The Geodes were controlled from a laptop in order to view each shot to ensure acceptable data quality, and record and process the data. Additional shots with the Peg-40 forming a new “stack” of data were added until the desired data quality was achieved. The shot record (seismogram) was also saved to the computer and stored for subsequent processing. A real-time noise monitor showing all geophones was carefully scrutinized during shots to ensure that noise levels were at a minimum for each shot. This included watching for breaks in wind noise, ATV traffic, and other sources of noise.

Table 2. Seismic Survey Details

Line Name	Date(s) of Acquisition	Direction of Collection	Geophone Spacing	Line Length
Line 1	9/7/2017 to 9/10/17	East to West	20 ft	3,820 ft
Line 4	9/11/2017, 9/12/17	West to East	20 ft	3,100 ft

3.1.3 Gravity Data Acquisition

Gravity data were acquired in one stage of field work from September 11th until September 17th, 2017. A total of 82 new gravity stations were established for this time period. Gravity data acquired from previous studies by various other entities existed within the site area and were incorporated during processing to provide regional gravity information. These data are publicly available at the University of Texas El Paso’s PACES website.

The gravity loop for the first day of acquisition (September 11th, 2017) was referenced to the base station located at the Blue Mist Hotel in Florence, Arizona. An absolute gravity was established there in October of 1969. Figure 5 shows the information regarding the base station’s location. A local base station, 3001, was established near the field survey area. Readings were taken at the beginning, middle and end of the day at the local base station to compensate for internal drift and for tide correction purposes. The absolute gravity for any particular station is obtained after removing the tide correction, meter drift and referencing the difference to a previously known base station.

Figure 5. Florence Absolute Gravity Base Station Information.

COUNTRY	TYPE OF STATION	STATION	
Arizona	base	Florence	
LOCATION	TYPE OF MARK	ESTABLISHED BY	GRAVITY VALUE (g)
Florence	BM reference	AMS	
LATITUDE	LONGITUDE	DATUM/REFERENCE	ELEV. (FT)
33° 01.8'N	111° 22.6'W	Florence 7.5'	1507

REMARKS Station site is located on NE corner of small retaining wall, approx. 50 ft. SW of intersecting c/l's of US Highways 80, 89 and state route 287.

ORDER | EST. BY | DATUM

DATE	OBSERVER	INSTRUMENT	BASE	BASE VALUE (g)	Δ g

H I=+00.3ft..

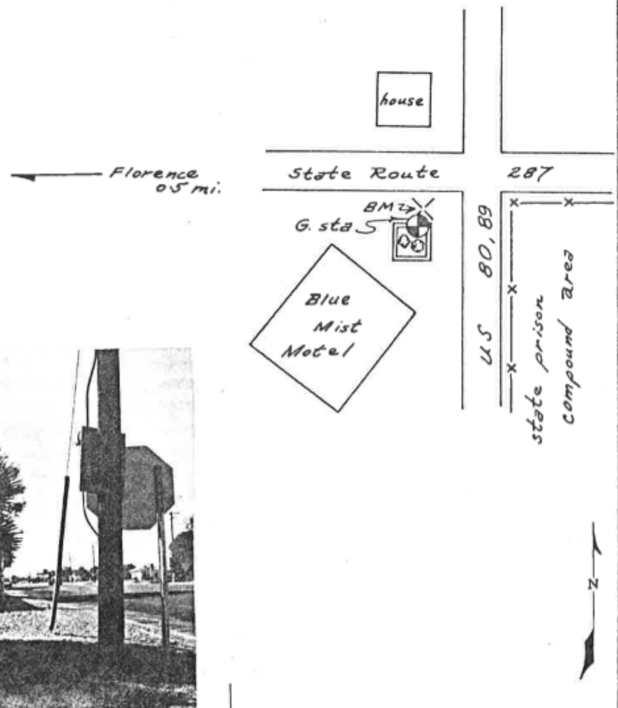

DATE OF PHOTO:

SKETCH

(Described) (Recovered) BY	AGENCY	DATE
C H Marcum	AMS	31 Oct. '67

DA FORM 1 OCT 64 2862 — DESCRIPTION OF GRAVITY STATION (TM 5-237)

3.2 EQUIPMENT

3.2.1 Resistivity Equipment

Data were collected using a Supersting™ R8 multichannel electrical resistivity system (Advanced Geosciences, Inc. (AGI), Texas) and associated cables, stainless steel electrodes, and battery power supply. The Supersting™ R8 meter is commonly used in surface geophysical projects and has proven itself to be reliable for long-term, continuous acquisition.

3.2.2 Seismic Equipment

Two Geode Ultra-Light Exploration 24–Channel Seismographs (Geometrics, Inc., San Jose, CA) were used for seismic P-wave refraction surveying, providing a total of 48-channels. 14Hz geophones were placed every 20 feet, and the seismic source consisted of the PEG-40.

3.2.3 Gravity Equipment

An Aliod LaCoste and Romberg Model G Geodetic Gravity Meter (S/N 400) was used for gravity data acquisition. The gravimeter has internal temperature compensation and is sealed to eliminate any effect from changes in the atmospheric pressure. The unit has a reading accuracy of ±.01 milligal and a drift rate of less than 1 milligal per month.

3.2.4 GPS

During resistivity and seismic field efforts, positional data were acquired via a handheld GPS; these data were used by the HGI field crew to record the location of survey lines and track survey progress, as well as produce preliminary model results. GPS locations for select resistivity electrodes and seismic stations were surveyed in greater detail and provided to HGI by the client; these GPS data were incorporated into the final coverage maps and the resistivity/seismic models presented in this report.

Gravity stations acquired for this investigation were located using a Garmin Etrex Vista hand-held GPS unit. Elevations were determined using digital elevation models (DEMs) and topographic sheet information.

3.3 QUALITY CONTROL

Data were given a preliminary assessment for quality control (QC) in the field to assure quality of data before progressing the surveys. Following onsite QC, all data were transferred to the HGI server for storage and detailed data processing and analysis. Data quality was inspected and checked for consistency with respect to adjacent results, and data files were saved to designated folders on the server. Records of survey configuration, location, equipment used, environmental conditions, proximal infrastructure or other obstacles, and any other useful information were recorded during data acquisition and were saved to the HGI Tucson server. The server is backed up nightly and backup tapes are stored at an offsite location on a weekly and monthly basis.

3.4 DATA PROCESSING

3.4.1 Resistivity Data Processing

The geophysical data for the resistivity survey, including measured voltage, current, measurement (repeat) error, and electrode position, were recorded digitally with the AGI SuperSting R8 resistivity meter. Quality control, both in-field and in-office, was performed throughout the survey to ensure data quality passed accepted standards. Data were assessed and data removal was performed based on degree of noise/other erroneous data. During data removal, those data that appeared to be extremely noisy and fell outside the normal range of accepted conditions were manually removed within an initial Excel spreadsheet analysis. Examples of conditions that would cause data to be removed include, negative or very low voltages, high-calculated apparent resistivity, extremely low current, and high repeat measurement error. No resistivity data values were manipulated or changed, such as with smoothing routines or box filters; noisy data were only removed from the general population. The edited dataset was then formatted for input to the 2D inverse modeling software.

3.4.1.1 2D Resistivity Modeling

RES2DINVx64 software (Geotomo, Inc.) was used for inverting individual lines in two dimensions. RES2DINV is a commercial resistivity inversion software package available to the public from www.geotomosoft.com. The inversion process followed a set of stages that utilized consistent inversion parameters to maintain consistency between each model. Inversion parameters were chosen to maximize the likelihood of convergence. Convergence of the inversion was judged whether the model achieved an RMS of less than 5% within three to five iterations. Inversion parameter choices included the starting model, the inversion routine (robust or smooth), the constraint defining the value of smoothing and various routine halting criteria that automatically determined when an inversion was complete. Qualified in-house inversion experts subjected each profile to a final review.

The inverted data were output from RES2DINVx64 and were gridded and color contoured in Surfer (Golden Software, Inc.). Where relevant and recorded, field observations such as roads, fences or other features were plotted on the resistivity section to assist in data analysis.

3.4.2 Seismic Data Processing

Data processing for the seismic refraction method consisted primarily of accounting for energy source and geophone locations, making adjustments for topographic changes along the geophone array profiles, and determining the first arrival times at the geophones. The final step was to determine subsurface acoustic properties using two different processing methods: refraction analysis, and tomographic inversion. The software incorporated all of the features necessary for accurate representation of subsurface properties, including the first break pick, inversion, and plotting.

Input Data: The geometry was created to define the relationship between the field file and channel numbers, and the source and receiver station numbers. Records marked in the Observer's logs as needing to be omitted were edited from the data. At this stage and within the software, edits and corrections were made to account for any errors made in the field.

First Arrival Selection: The first step for data processing was to pick the time for first arrival of energy at the geophone from each of the shot records, also known as first break picking. Each geophone had a separate first break pick for each shot. The first break picking was conducted interactively within the Seisimager's software called Pickwin Version 5.2.1.3.

Figure 6 shows an example shot record taken along Line 1. The x-axis is time in milliseconds and the y-axis is distance between geophones. The first break picks of energy arriving at the geophones are annotated as red marks below. There is an automatic picking option that is used initially in the software and then each trace in each shot record is manually reviewed and adjusted. In total there were 180 shot records and nearly 8,700 first break picks assigned. There were two distinct velocity slopes in arrivals representing the two layers as illustrated in Figure 6. The first slope, which is much steeper, indicates the slower velocity alluvium layer. The other layer is the refracted energy as it returns from the second and higher velocity layer. The second higher velocity layer was either a more consolidated alluvium or weathered bedrock.

Figure 6. Example Shot Record Showing First Break Picks.

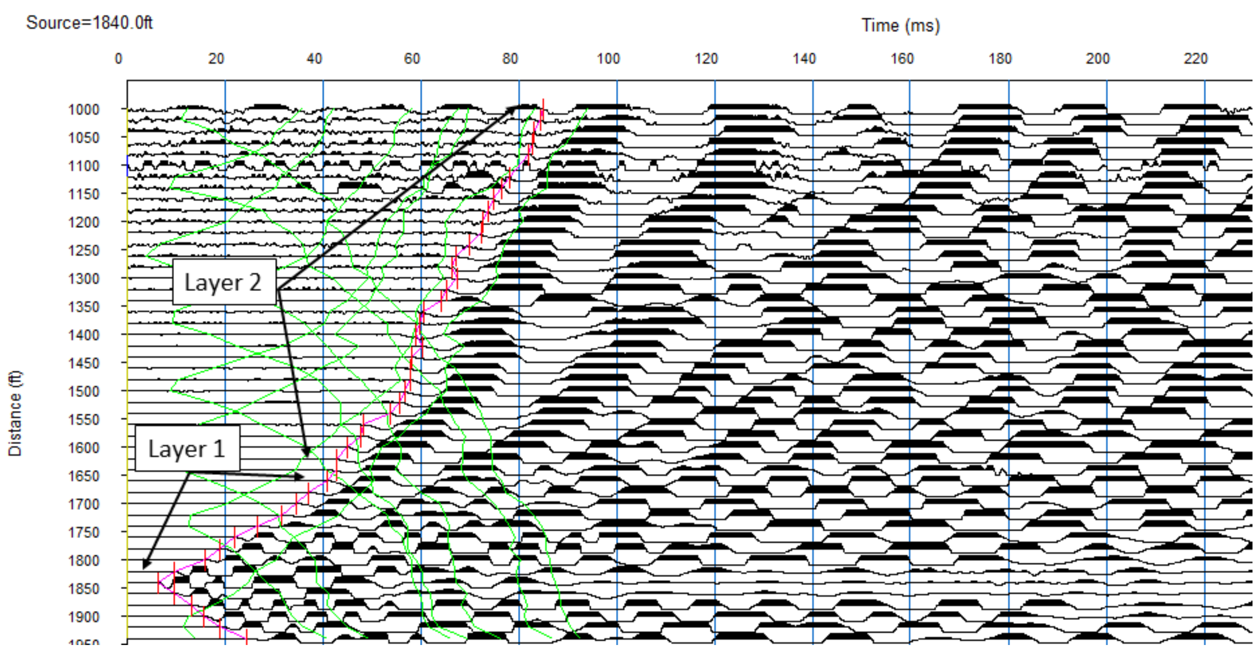

3.4.2.1 Seismic Refraction Modeling

Layer Assignment: Once the first breaks were assigned for all of the seismic lines, the next step in the process was layer assignment, where the user chose the slopes that best fit the two-layer or three-layer model. Figure 7 shows an example of the layer assignment chosen using SeisImager's software called Plotrefa Version 3.1.0.5. The x-axis now shows distance and the y-axis shows the time in milliseconds. The red circles represent Layer 1 and the green circles represent Layer 2.

Figure 7. Example of Layer Assignments (Line 4).

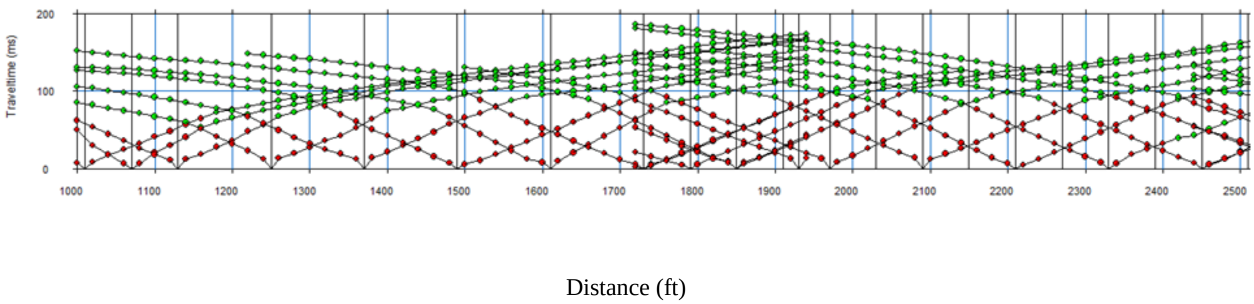

Refraction Analysis: Upon completion of the first break picks and the layer assignments, the refraction analysis was completed using the Seisimager software. Refraction analysis was completed for both lines using the time-term inversion modeling assuming a two or three layer model. An initial model was used for geometry verification. The refraction statics program compared the predicted pick times with the actual pick times producing numerous statistical displays used for finding and correcting shot/patch position errors. A two or three layer depth model was created using algorithms based on the generalized reciprocal method. This method assumes that layer velocity is constant and that the layer extends throughout the modeled section. For flat-layered geology this method is reliable and accurate, but tends to poorly represent variable horizontal velocity material and complex topographic changes within the layer.

Tomographic Inversion: Tomographic velocity inversion was completed using the Seisimager software. This method starts with an initial velocity model (generated manually or by the above mentioned time-term inversion and iteratively traces rays through the numerical model) with the goal of minimizing the root-mean squared (RMS) error between the observed and calculated travel times. Tomographic inversion is generally best suited for situations where velocity contrasts are known to be more gradational than discrete. In cases where strong horizontal velocity variations are known to exist, and in extreme topography, processing can lead to erroneous results with time-term least squares and delay-time inversion, depending on the severity of variations. Thus, tomographic inversion was chosen for the profiles here. The final output of the inversion modeling is a profile (X and Z dimensions) of acoustic velocity beneath each geophone spread. Generally, tomographic inversion requires a larger quantity and higher quality of data to produce viable results.

Table 3 shows the velocities of the layers as calculated by the time-term inversions. Each area tends to demonstrate differing properties for the calculated velocities for the layers. Line 1 indicates a second layer velocity of 6,000 ft/s, whereas Line 4 indicates a second layer velocity of 7,000 ft/s. Line 1 indicates a third layer with a velocity of 13,000 ft/s, but Line 4 does not indicate the presence of a third layer. These variations are most likely a consequence of the difference in surficial and bedrock geology across the site (Figure 8).

Table 3. Layer Velocities from Seismic Inversions

Line	Length (ft)	Layer 1 Velocity (ft/s)	Layer 2 Velocity (ft/s)	Layer 3 Velocity (ft/s)
1	3,820	2,000	6,000	13,000
4	3,100	2,000	7,000	N/A
Total	**6,920**			

3.4.3 Gravity Data Processing

Gravity data reduction includes the following steps:

- *Conversion from dial reading to milligals*. This conversion is made using calibration constants determined from the manufacturer of the instrument.

- *Removal of solid earth tidal effects*. The sun and moon have their own gravity fields that distort the Earth's gravity field. The same gravitational attraction that causes tidal effects with oceans also causes the solid earth to react to deformational forces caused by the gravitational pull of the sun and the moon. In simpler terms, the surface elevation rises and falls such that a correction must be made for the elevation differences during the course of the day. These effects are accounted for by applying calculated theoretical solid earth tide corrections, which are cyclical and predictable. It is important for the operator to record the date and time of measurement as data are acquired so that this correction can be completed.

- *Removal of instrumental drift*. Every meter suffers from some amount of instrumental drift caused by changes in the gravity meter's suspension system. Therefore, the operator must return to an established base station periodically and record several readings at this station so that the drift rate can be calculated and removed. The assumption is made that instrument drift is linear between base station readings.

- *Adjustment of milligal values to the regional base station value to produce absolute gravity values*. To this point, the data are arbitrary values and must be referenced to stations that have established absolute gravity values. This is completed by tying the field base station to one or more absolute gravity stations.

- *Removal of latitudinal effects*. There are two factors that contribute to the latitude correction. The Earth's rotation and its slightly oblate shape affect the gravitational pull as a function of latitude. The acceleration of the Earth's rotation is minimum at the poles and maximum at the equator. The 1967 Geodetic Reference System Equation (GRS 67) that accounts for latitudinal effects is given by:

$$g = 978{,}031.8461(1 + 0.005278895 \sin 2\Phi + 0.000023462 \sin 4\Phi)\ mGals$$

where Φ is the angle of latitude.

- C*orrection for elevation (Free Air Anomaly or FAA)*. This correction accounts for the decrease in gravity with an increase in elevation above the geoid. The free air correction is added to the observed gravity because the observed gravity would be lower at an elevation higher than the geoid surface. There is an approximate change of -0.096 milligal per foot due to elevation differences.

- *Correction for the Bouguer slab (Simple Bouguer Anomaly or SBA)*. This correction accounts for the attraction of earth material between a reference geoid surface and the individual station elevations. This is completed by treating the intervening material as an infinite horizontal slab, of a thickness equal to the elevation difference between the reference base and the individual station that has a uniform density. Generally, for the purpose of comparison to other gravity studies, this density is 2.67 g/cc, which is the mean crustal density.

- *Removal of terrain effects (Complete Bouguer Anomaly or CBA)*. Terrain corrections are necessary in areas of rough terrain or in relatively large areas of coverage where elevation differences are deemed substantial. Terrain corrections are completed with local elevation data using GPS equipment, as well as DEM information.

- *Removal of regional trends*. There are several commonly accepted procedures used for the removal of long-wavelength signatures caused by deep-seated isostatic compensation (crustal variations), which when removed enhance shallower features that are of interest to this investigation. The trend removal process produces Residual Bouguer Anomaly (RBA) values. The regional trend removed for this project is based on a linear trend for each gravity model, where the observed gravity values at exposed bedrock in either the Ruin Granite or the Teacup Granodiorite on the western and eastern ends of profiles were used to define the slope of the regional gradient. The gravity values along each profile were adjusted such that the slope was removed and the zero gravity value was established on both ends of the profile. Typically, a grid based approach is taken to remove the gradient from a gravity database; however, it is conditional on having a sufficient number of existing database gravity points to do so. Upon trying to remove a grid based regional gradient, it was deemed that there were not enough regional points outside of the survey area. For qualitative purposes the RBA map is shown and discussed in this report, but the gravity models are derived from the linear trend removal, which we feel to be more accurate.

Gravity data from previous surveys were imported into the working database. Some of these database points awere obtained from the University of Texas at El Paso Pan American Center for Earth and Environmental Studies. To ensure the proper merging of data from different surveys, all possible steps in the processing scheme were completed again using the same parameters. The two calculations, elevation and terrain, were recomputed for each database point prior to integration with HGI's September 2017 gravity data. A licensed version of RasterTC © from Geophysical Software was used for all terrain corrections using a search radius of 10 to 350 meters for the inner zone corrections and a search radius of 350 to 10,000 meters for the outer zone correction. A terrain density of 2.67 g/cc was used. The DEM used was obtained from the United States Geological Survey (https://viewer.nationalmap.gov).

3.4.3.1 Gravity Modeling

To determine relative depth to bedrock estimations, two-dimensional gravity modeling is required. The modeled profiles were developed using the following steps:

- The profiles were oriented to cross major gravity responses as orthogonally as possible (two-dimensional gravity modeling software must assume an infinite strike length of the modeled body in the third dimension).
- The contoured gravity responses along the chosen profile were digitized. Spacing varied along each profile depending on the gravity response. In areas of high gradient, the spacing is dense compared to minimal gradient areas.
- Elevation data from DEMs and gravity stations were used to develop a topographic surface. The DEMs were acquired from the United States Geological Survey website (https://viewer.nationalmap.gov /)
- The topography and gravity data were imported into the commercially available modeling package GM-SYS.
- Geologic data, consisting of known bedrock/alluvium contacts and density values of alluvium from geophysical logs, were incorporated into the model.
- A minimum vertex polygonal model is generated and, with the assigned densities, a theoretical curve is calculated and compared to the field data. Adjustments are made to the

vertices of the model until a reasonable fit is achieved between the theoretical and field data, while still using a geologically plausible model. The results were analyzed and revised as necessary.

4.0 BACKGROUND

4.1 GEOLOGY

Figure 8 shows a plan-view coverage map of the resistivity and seismic survey line locations, overlaying site geology. The geologic map (Cornwall, H.R., and Krieger, M.H.: U.S. Geological Survey GQ-1206, 1975) shows that the predominant lithologic units that the lines cross are alluvium, travertine, gravel, granodiorite, and granite. The intersections of lithologic boundaries, as digitized from Figure 8, are annotated on the resistivity profile results of Section 5.0 for analysis of corresponding electrical properties.

Figure 8. Geology at Resistivity and Seismic Line Locations.

Adapted using Cornwall, H.R., and Krieger, M.H.: U.S. Geological Survey GQ-1206, 1975.

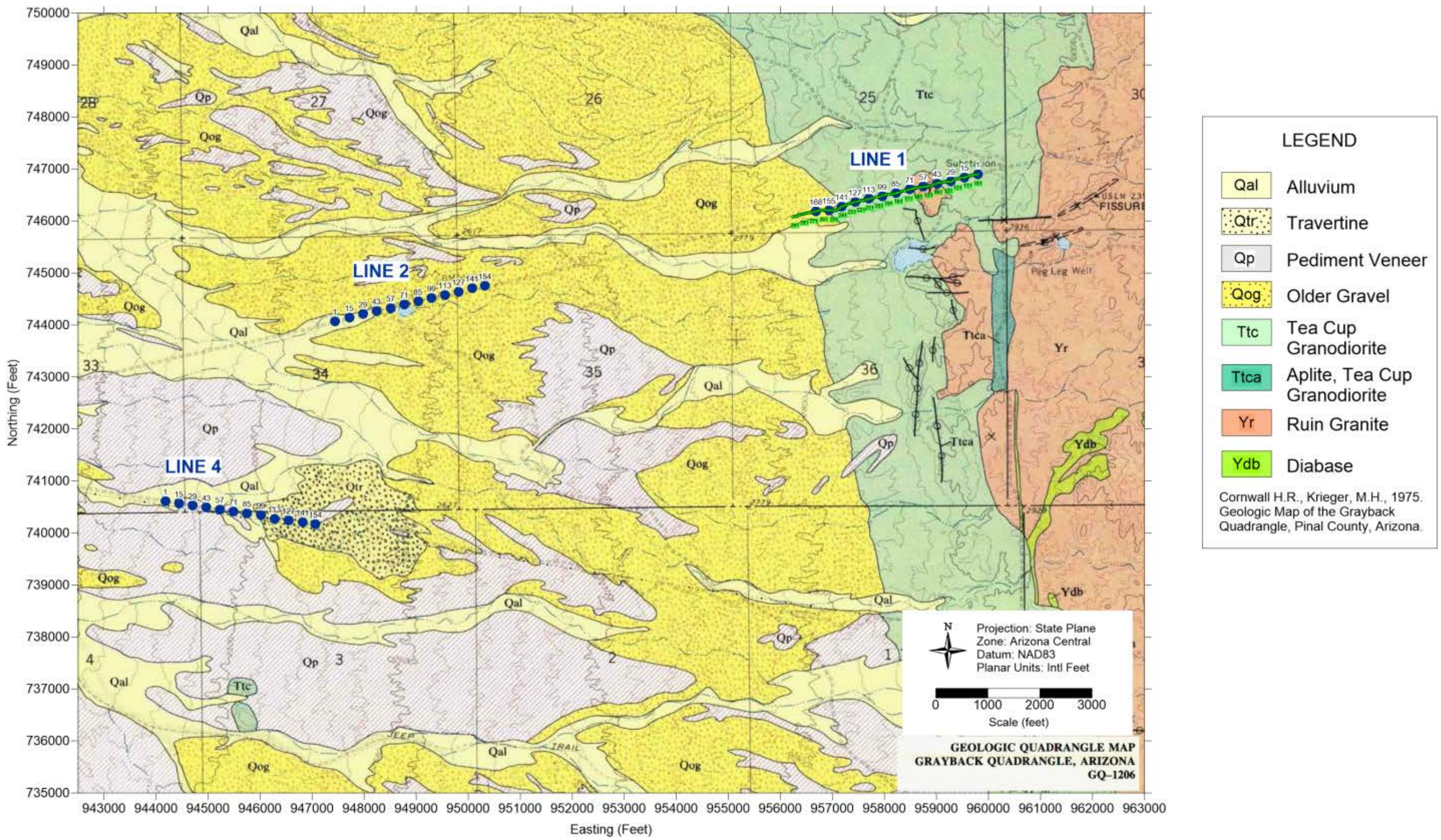

5.0 RESULTS & INTERPRETATION

The results of the three geophysical methods are first presented and discussed separately in the sections below, followed by a combined results discussion (Section 5.4).

5.1 ELECTRICAL RESISTIVITY RESULTS

The inverse model results are provided as two-dimensional (2D) profiles in the following section. Common color contouring scales are used for the lines to provide the ability to compare similar features from line to line, and a secondary color scale is then presented for Lines 2 and 4, to highlight any changes within a smaller data range. Electrically conductive (low resistivity) subsurface regions are represented by cool hues (purple to blue) and electrically resistive regions are represented by warm hues (yellow to brown).

Figure 9 shows results for all three resistivity lines, using the common color scale for grid contouring. As Figure 8 showed, the lines cross varying lithologic units and the resistivity results show evidence of the likewise varying electrical signature of these units. Figure 9A shows the results for Line 1, which the geology map indicates traverses more competent hard rock than Line 2 and 4, where we see higher resistivity features present to the center and west of the Line 1 profile. At the southwestern end of Line 1, the profile transitions to pink contours, indicating lower resistivity (higher conductivity). This also marks the lithologic transition to gravel material, which is the predominant surface unit mapped in the eastern portion of Line 2 as well (Figure 9B). Line 4 (Figure 9C) also shows resistivity values on the low end of the common color scale (the exception being a thin near-surface band of high resistivity over the western half of the profile). The geologic map shows Line 4 traversing surface-mapped travertine to the east, and gravel, sand and silt to the West. The individual line results are discussed in more detail in the following sections.

Figure 9. All 2D Resistivity Inverse Modeled Profiles (Common Color Scale).

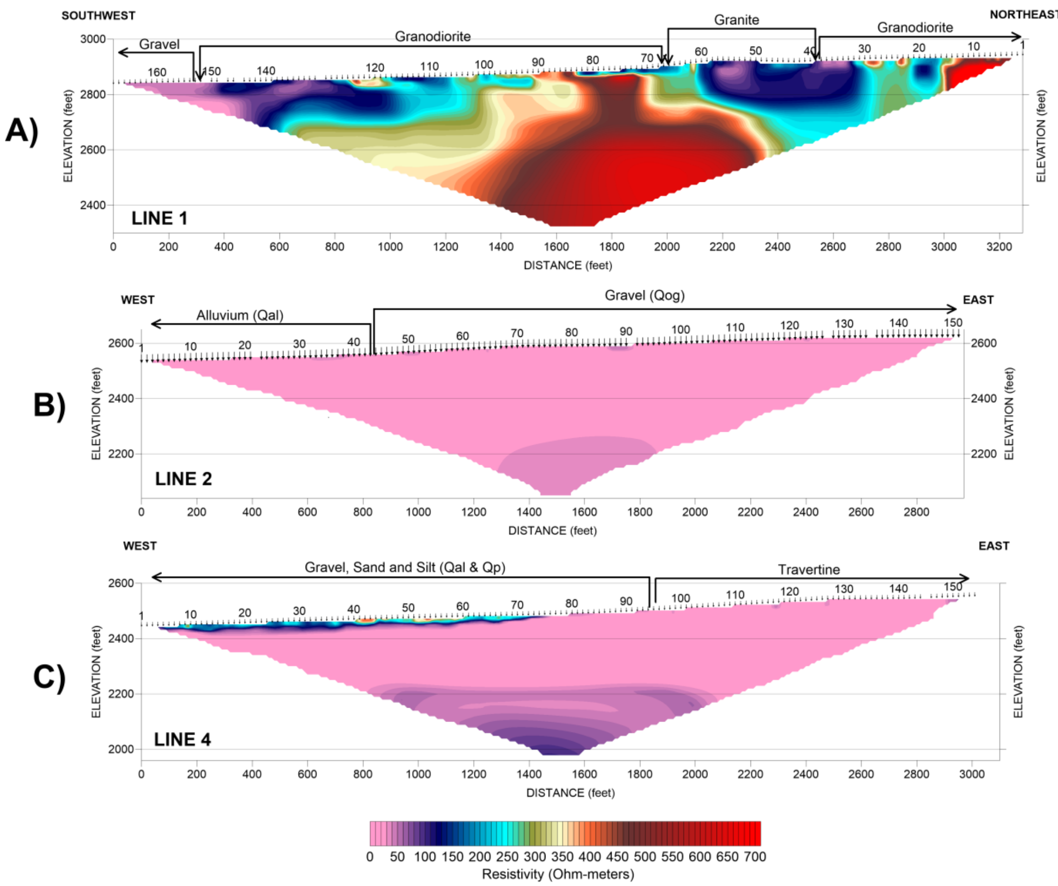

5.1.1 Line 1

Figure 10 presents the 2D inverse modeled profile for Line 1 resistivity data. Electrode numbers and lithologic transitions from Figure 8 are annotated on the top of the profile. The line was acquired from northeast to southwest in the field, but has been reversed to show southwest to northeast for ease of viewing and continuity with other line results.

As mentioned above, the line traverses granodiorite and granite, with a transition to gravel in the southwest. The gravel appears more conductive than the rest of the line, and the electrical signature of this unit correlates with resistivity vales for gravel observed in Line 2 to the west; values are generally in the 10-45 ohm-meter range. The granodiorite unit appears overall more resistive (exceeding 600 ohm-meters at the most resistive zone), while the granite body (which was noted in the field as outcropping between electrodes 49 and 70) appears conductive in comparison.

Figure 10. 2D Resistivity Inverse Modeled Profile – Line 1

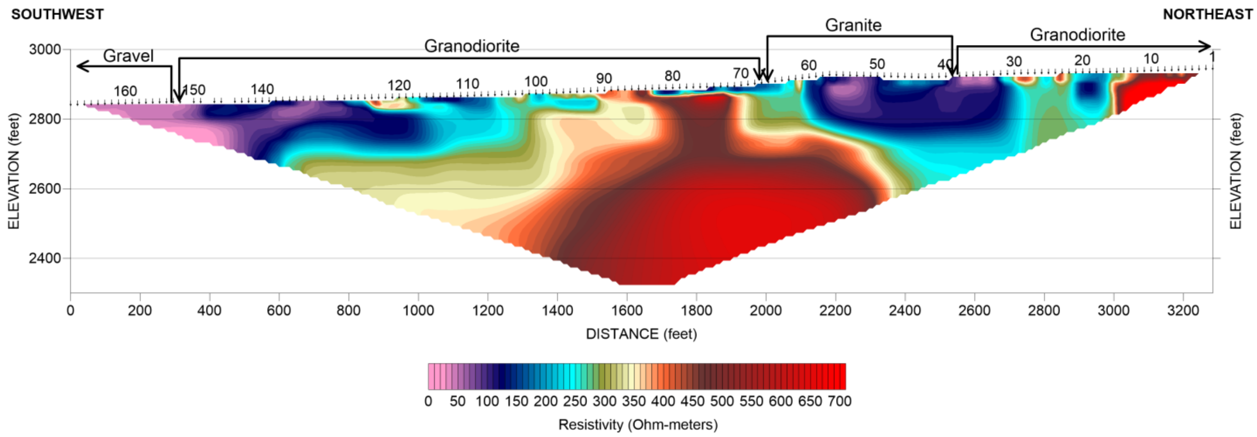

5.1.2 Line 2

Figure 11 presents the 2D inverse modeled profile for Line 2 resistivity data. Electrode numbers and lithologic transitions from Figure 8 are annotated on the top of the profile. The line was acquired from west to east and is located approximately 1.3 miles west of Line 1 (Figure 8). The color scale presented has been modified from the common color scale of Figure 9 to investigate heterogeneity within the smaller resistivity range in this area of the survey site.

Line 2 surface geology includes alluvium to the west and gravel to the east. The resistivity profile is generally conductive (<35 ohm-m), with some thin near-surface heterogeneity and a mild resistivity increase at depth.

Figure 11. 2D Resistivity Inverse Modeled Profile – Line 2

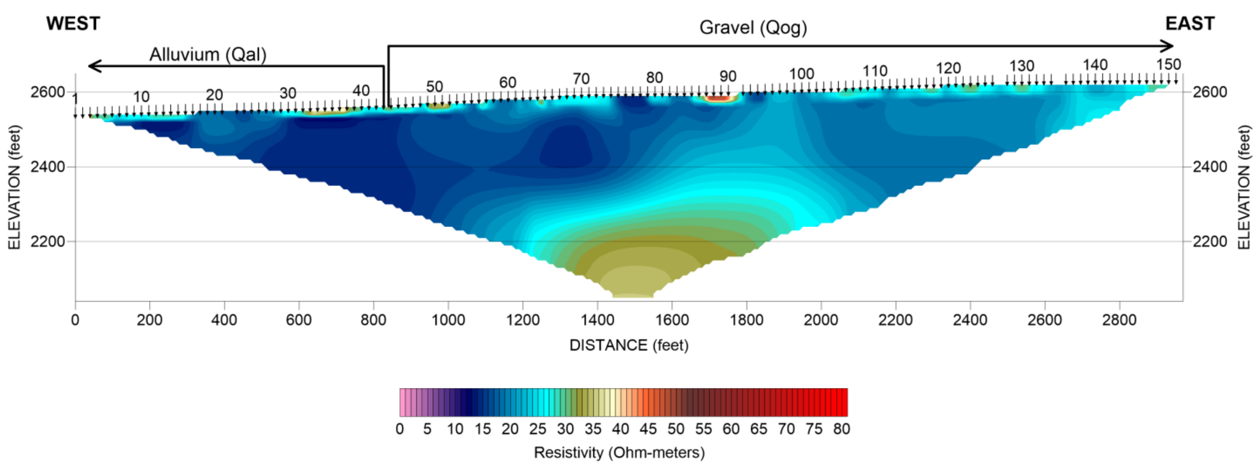

5.1.3 Line 4

Figure 12 presents the 2D inverse modeled profile for Line 4 resistivity data. Line 4 was located approximately .75 miles to the southwest of Line 2 (Figure 8). Electrode numbers and lithologic transitions from Figure 8 are annotated on the top of the profile. The line was acquired from west to east. The color scale presented has been modified from the common color scale of Figure 9 to investigate heterogeneity within the more conductive units in this area of the survey site, and is consistent with the focused scale of Line 2 in Figure 11.

Line 4 surface geology includes gravel, sand and silt to the west and travertine to the east. The resistivity profile shows a thin band of high resistivity on the western half of the line amongst the gravel, sand and silt (~20-40 foot thickness, 150-390 ohm-meters); the data were acquired along a road which may have higher resistivity due to material compaction. Below this resistive layer, and to the east, the data decrease in resistivity to ranges less than 30 ohm-meters (blue to purple contours). Beneath the surface-mapped travertine, some subtle layering is present in the electrical data, which may indicate layering or weathering, or even thickness, of this unit. There is a resistivity increase towards the deepest portion of the profile to values in the range of 40 to 90 ohm-meters.

Figure 12. 2D Resistivity Inverse Modeled Profile – Line 4

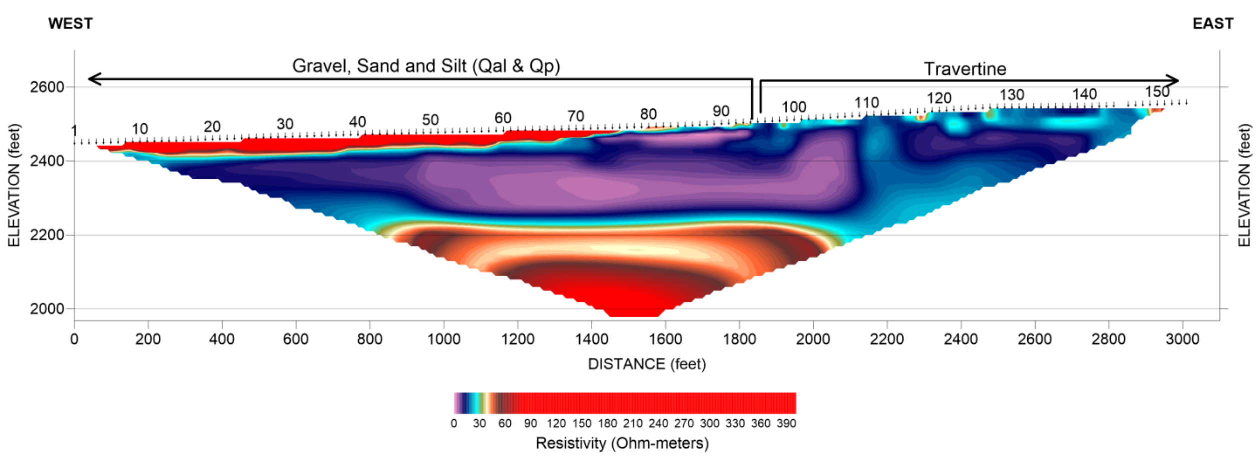

5.2 SEISMIC REFRACTION RESULTS

5.2.1 Line 1

Figure 10 presents the tomographic modeled profile for the Line 1 seismic refraction data. The velocities of the second and third layers from the time term inversion have been marked across the profile. The line was acquired from northeast to southwest in the field, but has been reversed to show southwest to northeast for ease of viewing and continuity with other line results. In general, locations where the tomographic contours become "tighter" usually indicate a sharper boundary between two materials. Locations where the tomographic contours spread out usually indicate a more gradual change or a more weathered material.

The depth to the top of the second and third layers is variable across the profile, but remains in the same general range for the eastern three-quarters of the profile. At about 1,000 feet from the western end of the profile the third layer dips noticeably deeper, and at about 850 feet from the western end of the profile the second layer dips noticeably deeper. This indicates that the bedrock is getting deeper in the western portion of the line, coincident with the presence of the quaternary gravel deposits that appear to be thickening to the west.

Figure 13. 2D Seismic Modeled Profile – Line 1

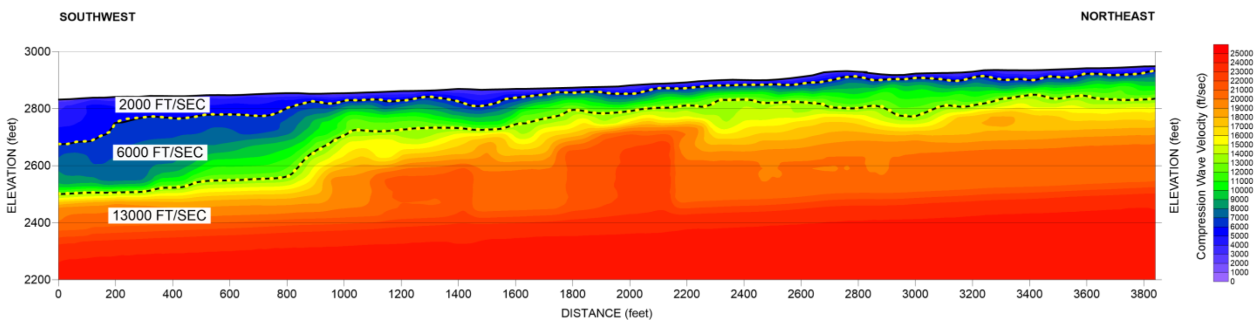

5.2.2 Line 4

Figure 10 presents the tomographic modeled profile for the Line 4 seismic refraction data. Line 4 is located approximately 1.8 miles southwest of Line 1. The velocity of the second layer from the time term inversion has been marked across the profile.

The depth to the top of the second layer is generally about 50 to 60 feet in the eastern portion of the profile, coincident with the location of the travertine deposit. Around 1,800 feet from the west end of the line, coincident with the quaternary alluvium deposits, the second layer dips down to a maximum depth of around 150 feet bgs around 1,650 feet from the west end of the line. The second layer then gets gradually shallower to the west, until it is about 60 feet deep at the west end of the line. The lack of a third layer refractor along Line 4 suggests that the more competent bedrock is deeper than in the area of Line 1.

Figure 14. 2D Seismic Modeled Profile – Line 4

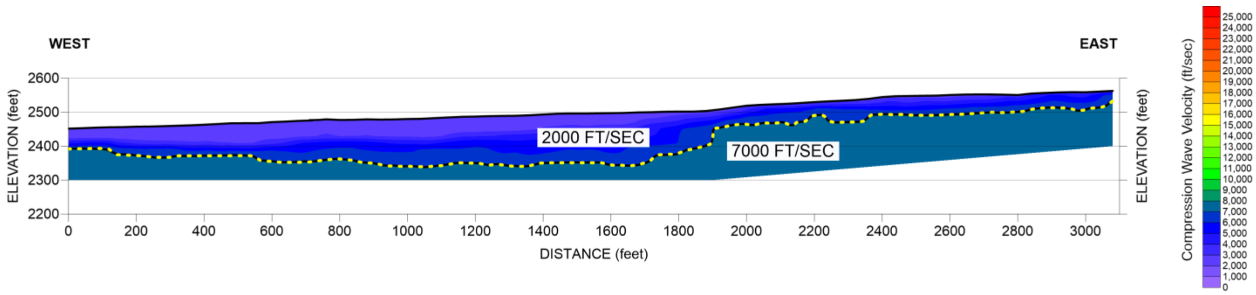

5.3 GRAVITY RESULTS

For the purposes of the gravity study, bedrock is defined as any pre-Cenozoic, crystalline or consolidated sedimentary rocks underlying the Tertiary and Quaternary basin-fill sediments.

For all plan-view plots, geographic coordinates are presented using the NAD83 State Plane Central Arizona datum with units in International Feet.

Figure 15, Figure 16, and Figure 17 show the various gravity maps created during the processing phase with the Digital Elevation Model (DEM) for the area used as an underlay. The proposed Peg Leg footprint is outlined in black. Regarding the color scale for the CBA and RBA values, red hues represent shallow bedrock near the surface, while green to blue hues represent thickening sequences of low-density alluvial fill. The modeled results for the three gravity models are displayed in Figure 18 through Figure 23.

5.3.1 CBA and RBA Interpretation

HGI’s interpretation is based upon the gravitational trends evident in the CBA and RBA plots, the modeled gravity profile results, and correlation with geologic information.

Referring to Figure 15, CBA values range from -61 to -41 milligals. It is counterintuitive to see the mountains in the eastern half of this figure form a gravity low while the western outcrops form a gravity high response. In actuality, there is a very long wavelength trend that relates to density changes many kilometers below in the earth’s crust. Figure 16 shows the CBA map for Arizona and illustrates how this regional trend is pervasive across the entire state. In the northern part of Figure 15, the CBA gravity contours do not show closure; this may be of significance to the overall study for the TSF placement.

This regional trend is removed before the modeling process can begin and is described in the report under the data processing section (Section 3.4.3).

Figure 17 shows a focused perspective of the RBA values around the Peg Leg survey area, with the locations of the three gravity profiles A, B and C, as well as the proposed footprint. The RBA values now range from 0 to -5 milligals. As expected, the highest RBA values (shown in red hues) are observed along the western and eastern outcrops where the Ruin Granite is exposed. The lower values, indicated in purple hues, represent greater depth to bedrock.

A notable feature in the RBA map is observed along the location of gravity model A-A', where there appears to be a gravity ridge that corresponds to the NW corner of the proposed TSF. This ridge separates the basin into two sections: a notable gravity low towards the north, where Gravy Model C is displayed, and a gravity low to the south, as seen between Gravity Models A and B.

In the northern portion of Figure 17, the RBA contours indicate some closure. This is in slight contradiction to the CBA contours, which show no closure of contours. This appears to be due to lack of gravity data to the north of the survey area, and warrants additional data collection and/or drilling to the northern part of this basin to confirm that bedrock may be as deep as it is currently hypothesized near the proposed TSF.

For all modeled cross-sections, the upper pane represents the gravity response along the chosen profile orientation. The lower pane represents the modeled geologic section. The vertical exaggeration for all models is 1.73.

Each of the models are oriented west to east beginning in the basin and terminating in the Precambrian rocks exposed to the east.

For the three models, HGI used the following densities for the main lithologies within the focus study area, and . Density units are in grams per cubic centimeter (g/cc).

- Basin fill – density of 2.00 g/cc and 2.35 (g/cc)
- Bedrock – density of 2.67 g/cc

The basin fill densities listed above were derived from other surveys completed by HGI in similar basins. Confirmation drilling from the Far West campaign in 2012 helped refine HGI's gravity models that were completed in Far West 2010 Report. The predictions for the modeled depth to bedrock indicated that bedrock was shallower than what was drilled. During the drilling, thick and dense volcanic layers were intercepted, which required a greater alluvial density to be used in the models to match the known depths to bedrock. That density was 2.35 g/cc and is used in the current gravity survey efforts to propose a second set of modeled depths to bedrock. Any deviation in the assumed densities has direct implications for our predicted depths to bedrock. If, for example, the basin fill is less dense than the assumed value, then the depths to bedrock will be overestimated. If alluvial densities are higher than the assumed value, then the depths to bedrock will be underestimated. Any deviations in the recognized average density for bedrock material

(2.67 g/cc) will also affect the predicted depths.

Upon any subsequent drilling, the models presented in this report may be refined by constraining the models to encountered drilled depths to bedrock. The refined set of models will then provide a more accurate understanding of the modeled depths to bedrock.

Figure 15. Complete Bouguer Anomaly.

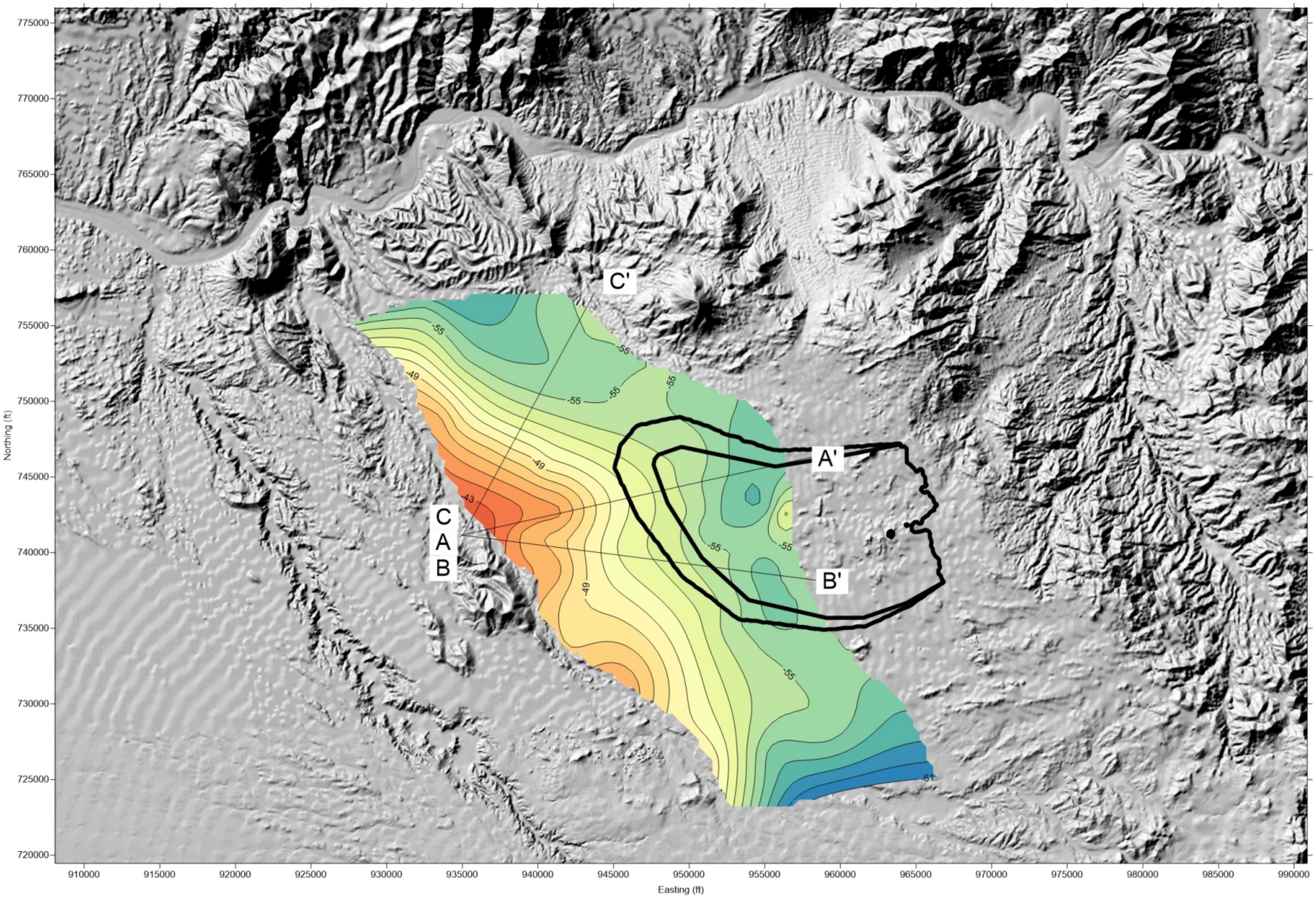

Figure 16. Complete Bouguer Anomaly for Arizona.

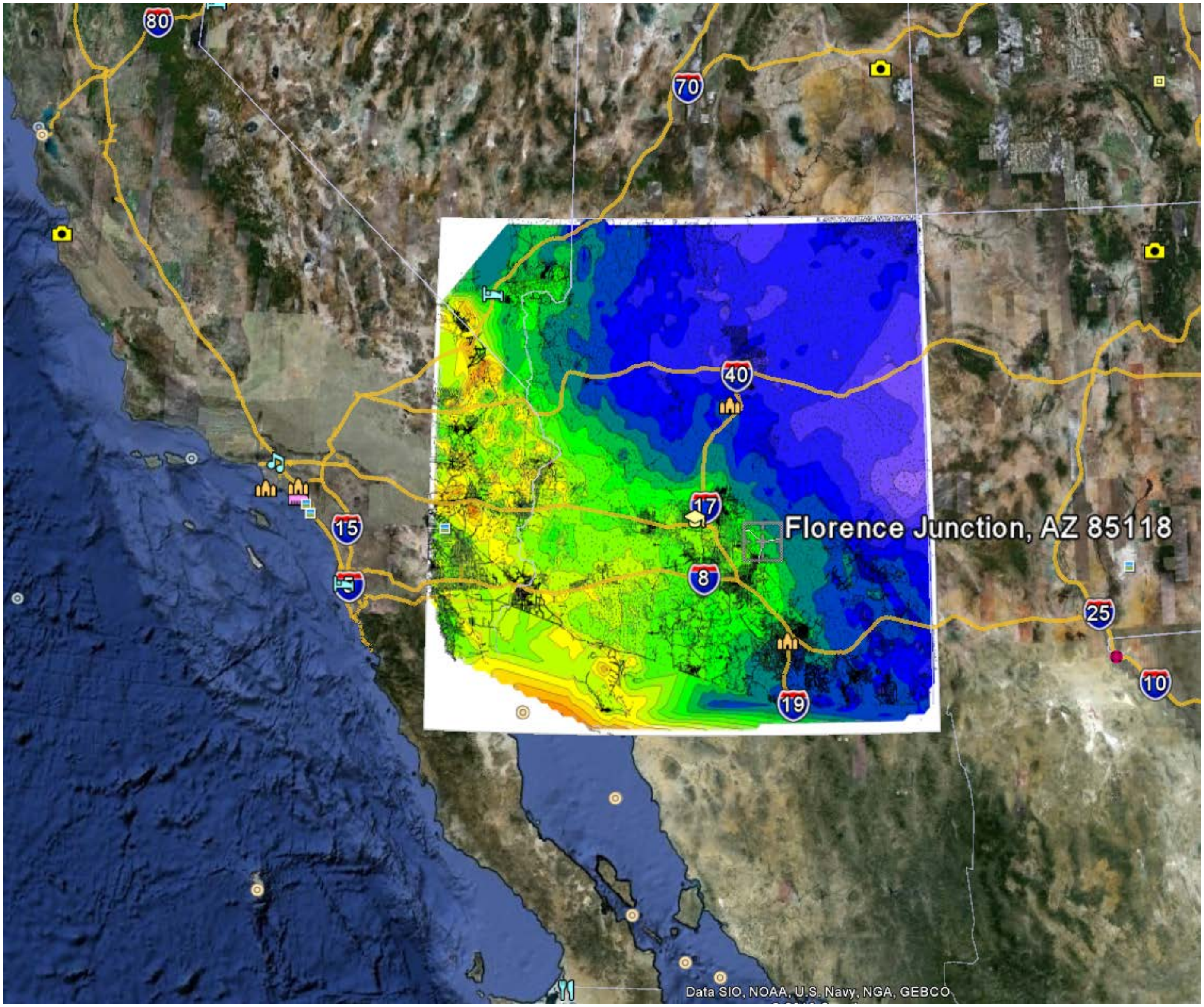

Figure 17. Focused Residual Bouguer Anomaly.

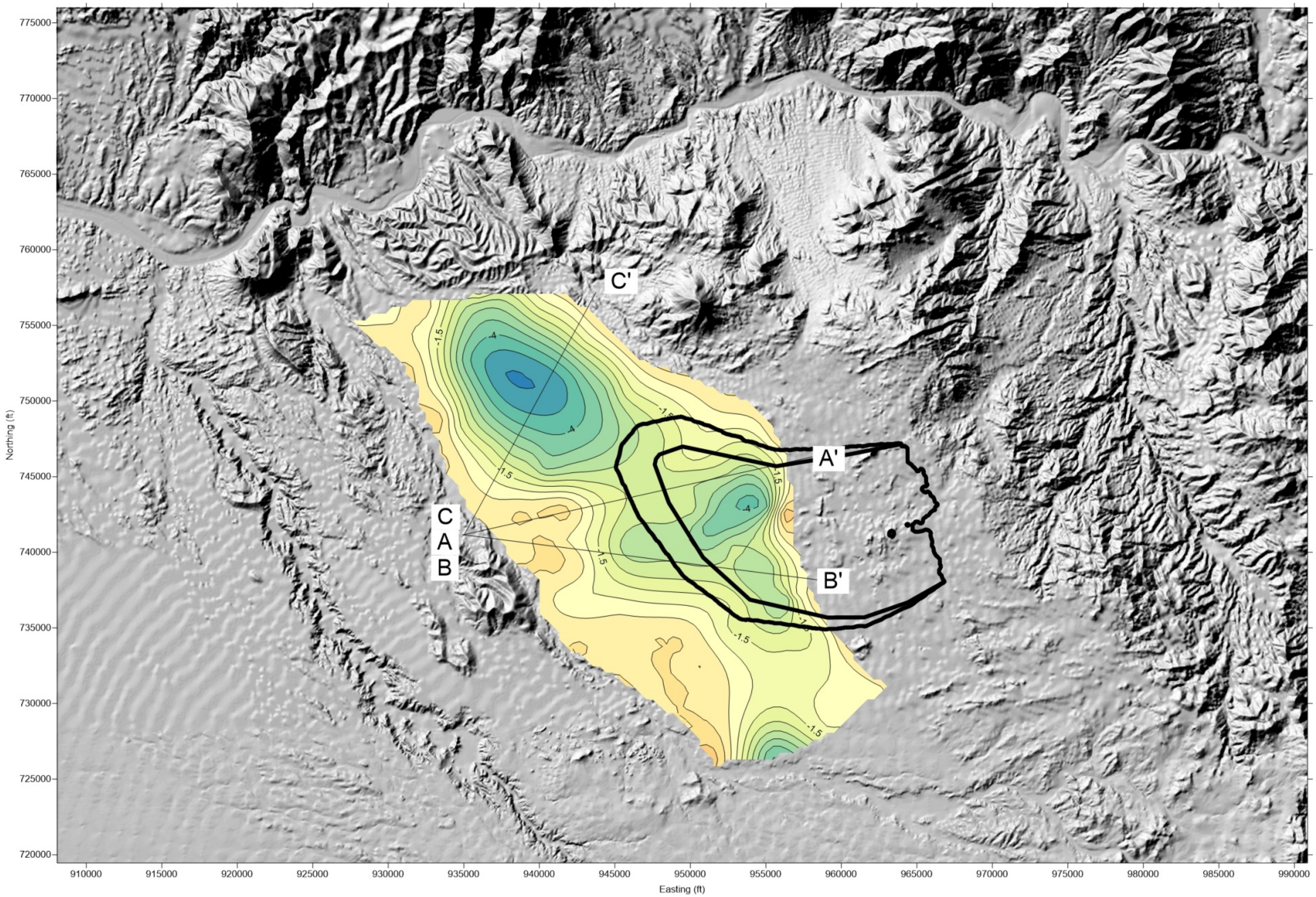

5.3.2 A-A' Gravity Profile

The A-A' gravity profile is shown in Figure 18 and Figure 19 using two different densities for the basin fill material, 2.00 and 2.35 g/cc, respectively. The RBA values range between 0 and -4 milligals. This profile is 4.5 miles long and has a heading of 77 degrees with the view looking north.

The modeled depths to bedrock for the two different alluvial densities are presented in Table 4. There is a large difference in the modeled depths to bedrock between the two different basin fill density models. The 2.00 g/cc is a realistic model unless there are buried dense volcanic units similar to what was intercepted at the Far West site in the 2012 drilling campaign. In which case, the depths to bedrock will likely resemble modeled depths to bedrock as shown for 2.35 g/cc basin fill density model. If drilling is performed that intercepts bedrock, the gravity models can be constrained to the intercepted depth to bedrock and propagated to the other models.

The modeled depths to bedrock appear to extend out into the basin from the exposed outcrop on the western side of the basin. Nominally, the modeled depths to bedrock in the deepest part of the basin for the two different basin fill models are about 600 ft bgs and 1,300 ft bgs respectively.

5.3.3 B-B' Gravity Profile

The B-B' gravity profile is shown in Figure 20 and Figure 21 using two different densities for the basin fill material, 2.00 and 2.35 g/cc, respectively. The RBA values range between 0 and -4 milligals. This profile is 4.5 miles long and has a heading of 77 degrees with the view looking north.

The modeled depths to bedrock for the two different alluvial densities are presented in Table 5. The gravity gradients and the modeled depths to bedrock are fairly symmetric on the western and eastern flanks of the basin. The eastern flanks appear to be slightly steeper, which is typical of basin and range environments. The basin floor flattens out between 1.5 and 3.4 miles along the profile. Nominally, the modeled depths to bedrock in the deepest part of the basin for the two different basin fill models are about 600 ft bgs and 1,300 ft bgs respectively.

5.3.4 C-C' Gravity Profile

The C-C' gravity profiles are shown in Figure 22 and Figure 23 using two different densities for the basin fill material, 2.00 and 2.35 g/cc, respectively. The RBA values range between 0 and -4.5 milligals. This profile is 3 miles long and has a heading of 28 degrees with the view looking northwest.

The modeled depths to bedrock for the two different alluvial densities are presented in Table 6. If drilling is performed that intercepts bedrock, the gravity models can be constrained to the intercepted depth to bedrock and propagated to the other models.

The eastern flanks of the model appear to be slightly steeper, which is typical of basin and range environments. The basin floor flattens out between 1.5 and 2.5 miles along the profile and, relative to the other profiles, the basin floor is not as wide. However, the modeled depths to bedrock are deeper than those in the A-A' and B-B' models. Nominally, the modeled depths to bedrock in the deepest part of the basin for the two different basin fill models are about 700 ft bgs and 1,550 ft bgs respectively.

Figure 18. Gravity Model A-A' using 2.00 g/cc for Basin Fill Density.

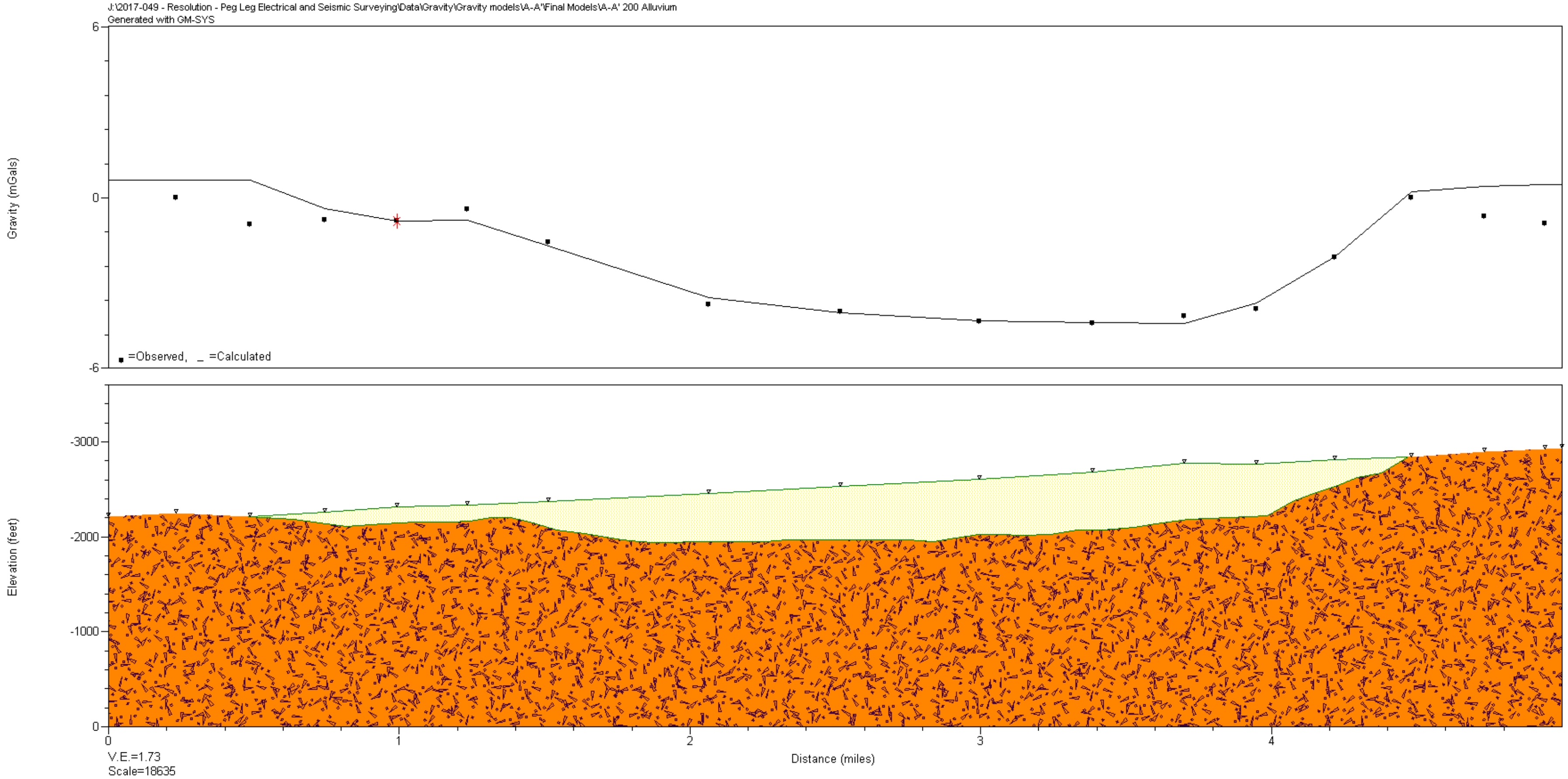

Figure 19. Gravity Model A-A' using 2.35 g/cc for Basin Fill Density.

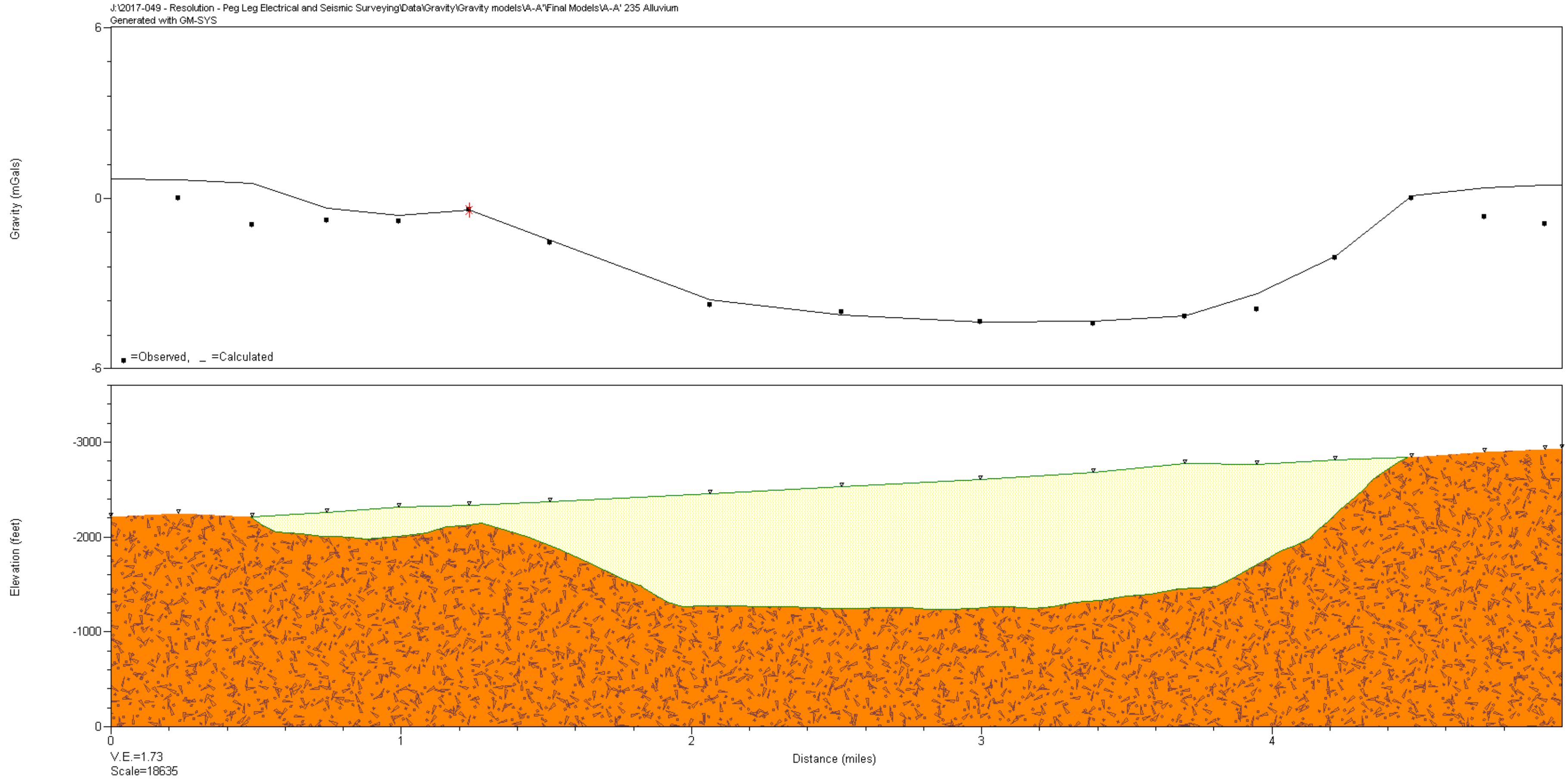

Table 4. Predicted Depths to Bedrock for A-A'.

Downline Distance (miles)	Depth to Bedrock (ft) 2.0 g/cc model	Depth to Bedrock (ft) 2.35 g/cc model
0	9	9
0.16	93	213
0.24	136	275
0.34	184	279
0.47	186	319
0.57	176	316
0.69	183	234
0.76	176	221
0.84	161	255
0.9	162	291
0.97	225	383
1.06	328	526
1.16	388	675
1.23	425	778
1.29	473	881
1.35	490	971
1.4	510	1040
1.45	520	1149
1.55	521	1196
1.64	533	1200
1.71	546	1213
1.78	554	1234
1.85	555	1250
1.93	573	1284
2	577	1298
2.05	592	1298
2.12	597	1316

Downline Distance (miles)	Depth to Bedrock (ft) 2.0 g/cc model	Depth to Bedrock (ft) 2.35 g/cc model
2.19	617	1328
2.27	629	1341
2.36	654	1364
2.44	632	1384
2.52	616	1389
2.59	619	1380
2.67	648	1395
2.76	653	1418
2.86	618	1377
2.94	628	1366
3.05	624	1345
3.13	589	1320
3.24	561	1292
3.31	567	1280
3.38	558	1280
3.51	579	1038
3.6	429	902
3.67	364	813
3.76	285	544
3.83	217	466
3.91	182	182
4.01	22	22

Figure 20. Gravity Model B-B' using 2.00 g/cc for Basin Fill Density.

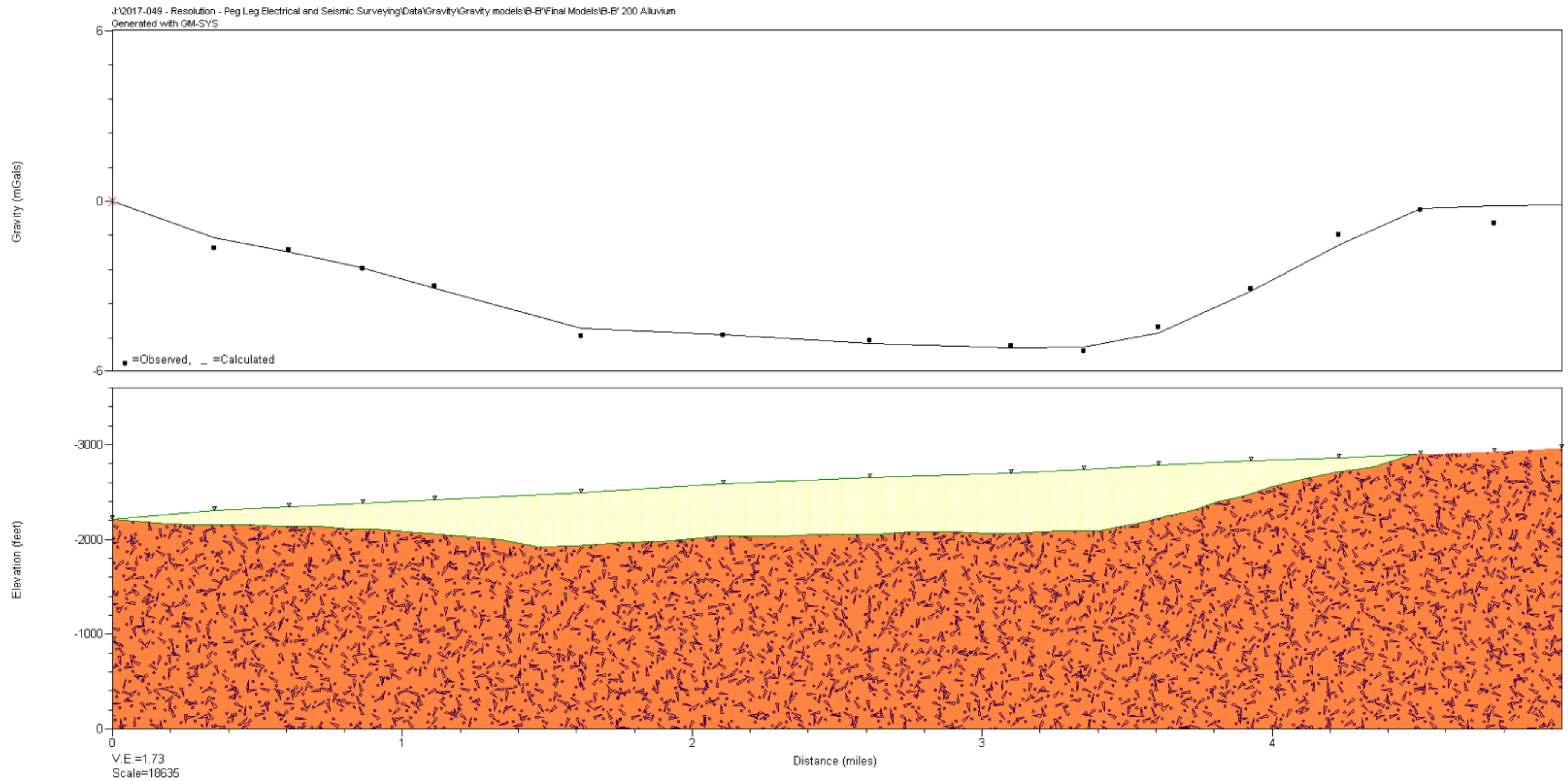

Figure 21. Gravity Model B-B' using 2.35 g/cc for Basin Fill Density.

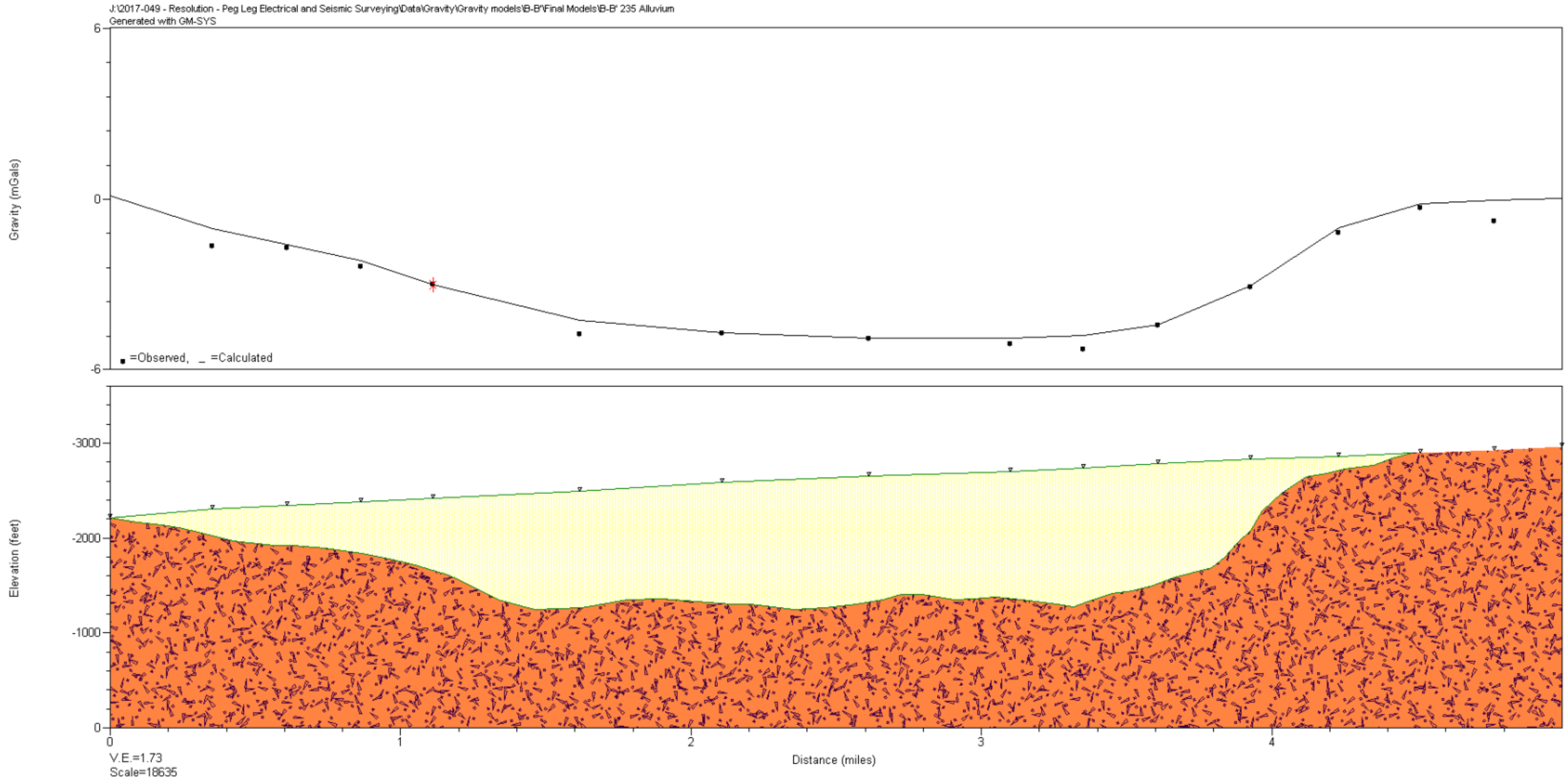

Table 5. Predicted Depths to Bedrock for B-B'.

Downline Distance (miles)	Depth to Bedrock (ft) 2.0 g/cc model	Depth to Bedrock (ft) 2.35 g/cc model
0	23	23
0.2	95	121
0.29	115	161
0.39	75	223
0.47	89	272
0.58	125	335
0.71	164	351
0.83	194	404
0.91	200	463
0.99	226	538
1.09	295	614
1.21	328	745
1.35	387	1037
1.47	482	1037
1.61	495	1155
1.77	482	1165
1.9	486	1106
2	476	1109
2.09	463	1158
2.21	482	1201
2.32	499	1230
2.43	505	1293
2.55	531	1302
2.65	551	1293
2.76	538	1207
2.84	541	1217
2.91	561	1257

Downline Distance (miles)	Depth to Bedrock (ft) 2.0 g/cc model	Depth to Bedrock (ft) 2.35 g/cc model
3.02	594	1293
3.12	597	1286
3.21	604	1348
3.29	594	1378
3.41	607	1368
3.55	545	1276
3.65	482	1234
3.74	436	1152
3.83	358	1073
3.91	308	961
4.02	223	699
4.13	154	315
4.24	95	154
4.37	72	89

Figure 22. Gravity Model C-C' using 2.00 g/cc for Basin Fill Density

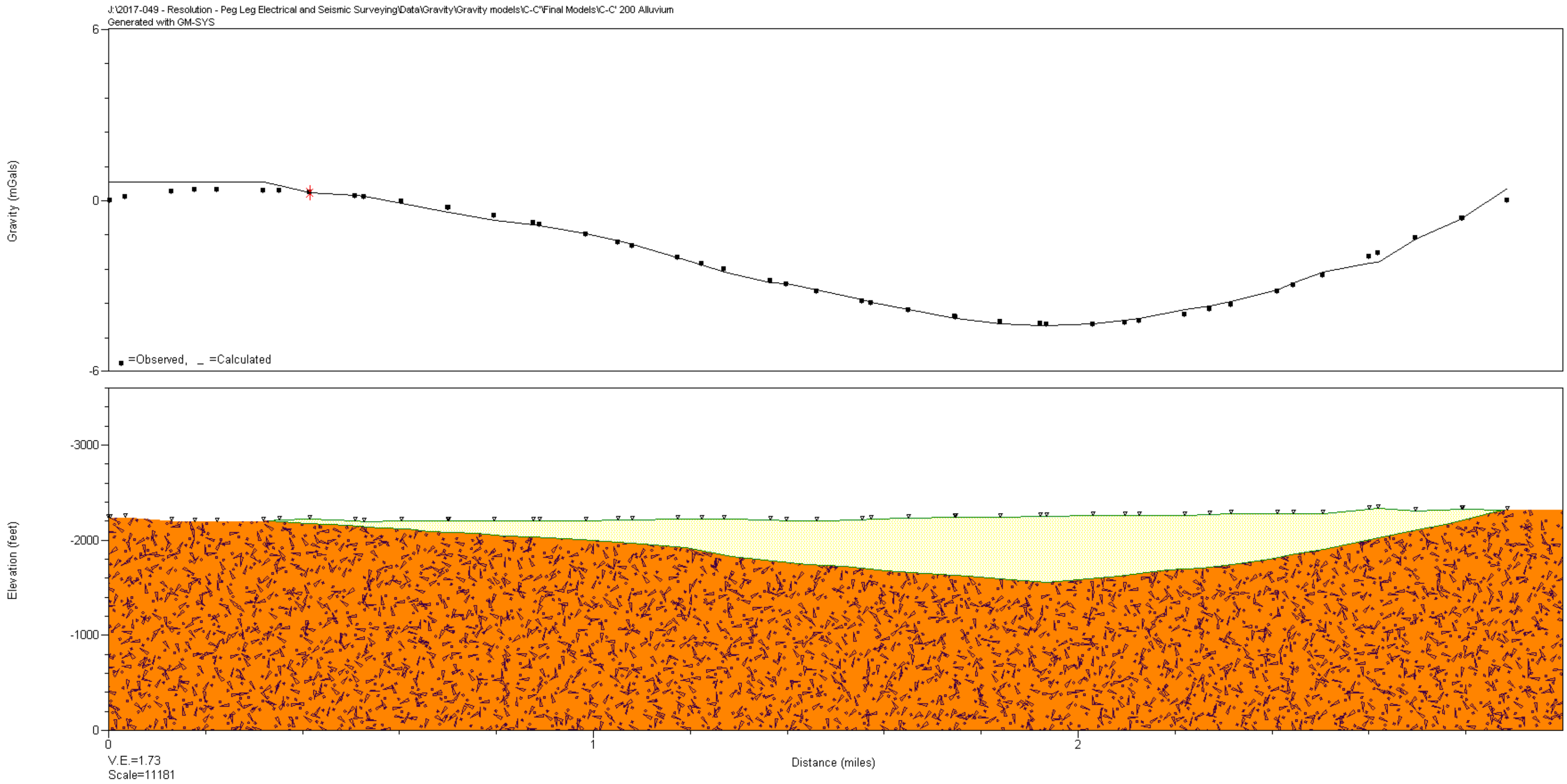

Figure 23. Gravity Model C-C' using 2.35 g/cc for Basin Fill Density

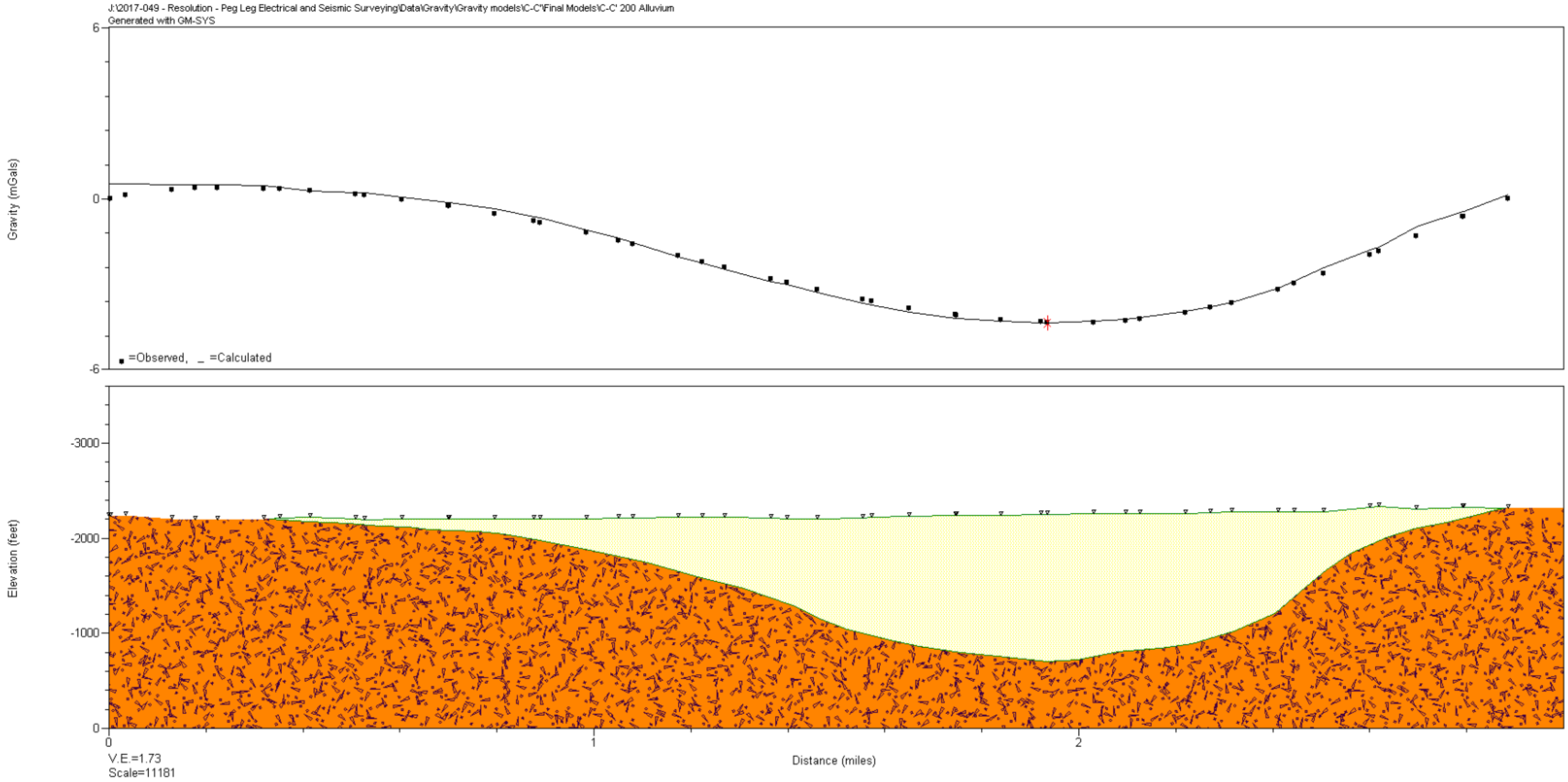

Table 6. Predicted Depths to Bedrock for C-C'.

Downline Distance (miles)	Depth to Bedrock (ft) 2.0 g/cc model	Depth to Bedrock (ft) 2.35 g/cc model
0	0	0
0.08	39	0
0.16	46	39
0.23	69	69
0.29	85	85
0.33	108	85
0.38	121	121
0.43	135	135
0.48	161	135
0.54	167	161
0.65	200	220
0.77	253	331
0.86	305	472
0.96	390	623
1.03	433	751
1.12	459	912
1.19	486	1066
1.28	541	1165
1.36	584	1306
1.45	620	1371
1.54	659	1447
1.61	696	1493
1.68	666	1545
1.76	636	1526
1.86	571	1460
1.93	558	1421
2	528	1378

Downline Distance (miles)	Depth to Bedrock (ft) 2.0 g/cc model	Depth to Bedrock (ft) 2.35 g/cc model
2.07	479	1250
2.13	420	1073
2.19	377	827
2.24	338	827
2.31	315	614
2.38	210	453
2.44	138	341
2.5	95	210
2.55	43	138
2.57	10	138

5.4 COMBINED GEOPHYSICAL RESULTS

Figure 24, Figure 25, and Figure 26 show combined geophysical results for co-located model results for Lines 1, 2 and 4, respectively. Seismic velocity layers and data points from gravity models for depth to bedrock are overlain on the contoured resistivity profiles for comparison.

5.4.1 Line 1

Line 1 combined results incorporates all three geophysical methods (Figure 24). As mentioned above, the line traverses granodiorite and granite, with a transition to gravel in the southwest. The gravel appears more conductive than the rest of the line, and the seismic layer dips and follows along with the boundary of this conductive zone to the southwest. The gravity data also show a deepening of bedrock in the western portion of the line, coincident with the presence of the quaternary gravel deposits that appear to be thickening to the west.

5.4.2 Line 2

Line 2 combined results incorporates resistivity and gravity methods; no seismic data were acquired at this location (Figure 25). Line 2 surface geology includes alluvium to the west and gravel to the east. The resistivity profile shows a mild resistivity increase at depth, and the gravity data imply bedrock below the imaging depth of the resistivity profile, at varying depths depending on model parameters.

5.4.3 Line 4

Line 4 combined results incorporates all three geophysical methods (Figure 26). Line 4 surface geology includes gravel, sand and silt to the west and travertine to the east. In the eastern portion of the profile, beneath the surface-mapped travertine, the seismic show the depth to the top of the second layer is generally about 50 to 60 feet; the resistivity data show some horizontal layering at this location that is in agreement with the seismic layer.

There is a resistivity increase towards the deepest portion of the resistivity profile. The lack of a third layer refractor in the seismic data suggests that the more competent bedrock is deeper here than the seismic method imaged, and the gravity data show depths to bedrock below at 2000ft or below, which is below the imaging depth of both resistivity and seismic methods.

Figure 24. Combined Geophysical Results for Line 1: A) Seismic and Gravity (Density = 2.0 g/cc and 2.35 g/cc), B) Resistivity, Seismic, and Gravity (Density = 2.0 g/cc and 2.35 g/cc).

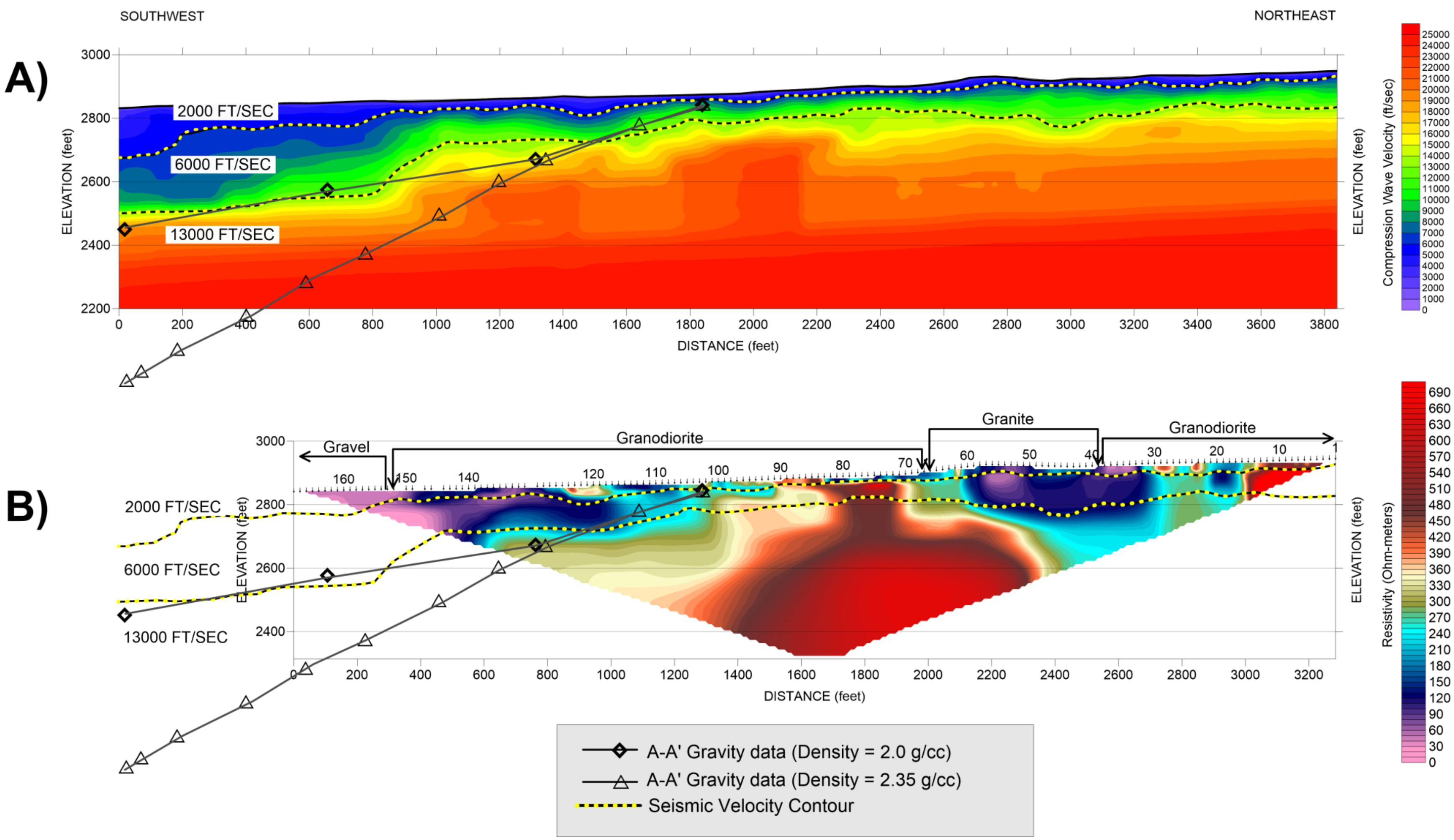

Figure 25. Combined Geophysical Results for Line 2: Resistivity and Gravity (Density = 2.0 g/cc and 2.35 g/cc).

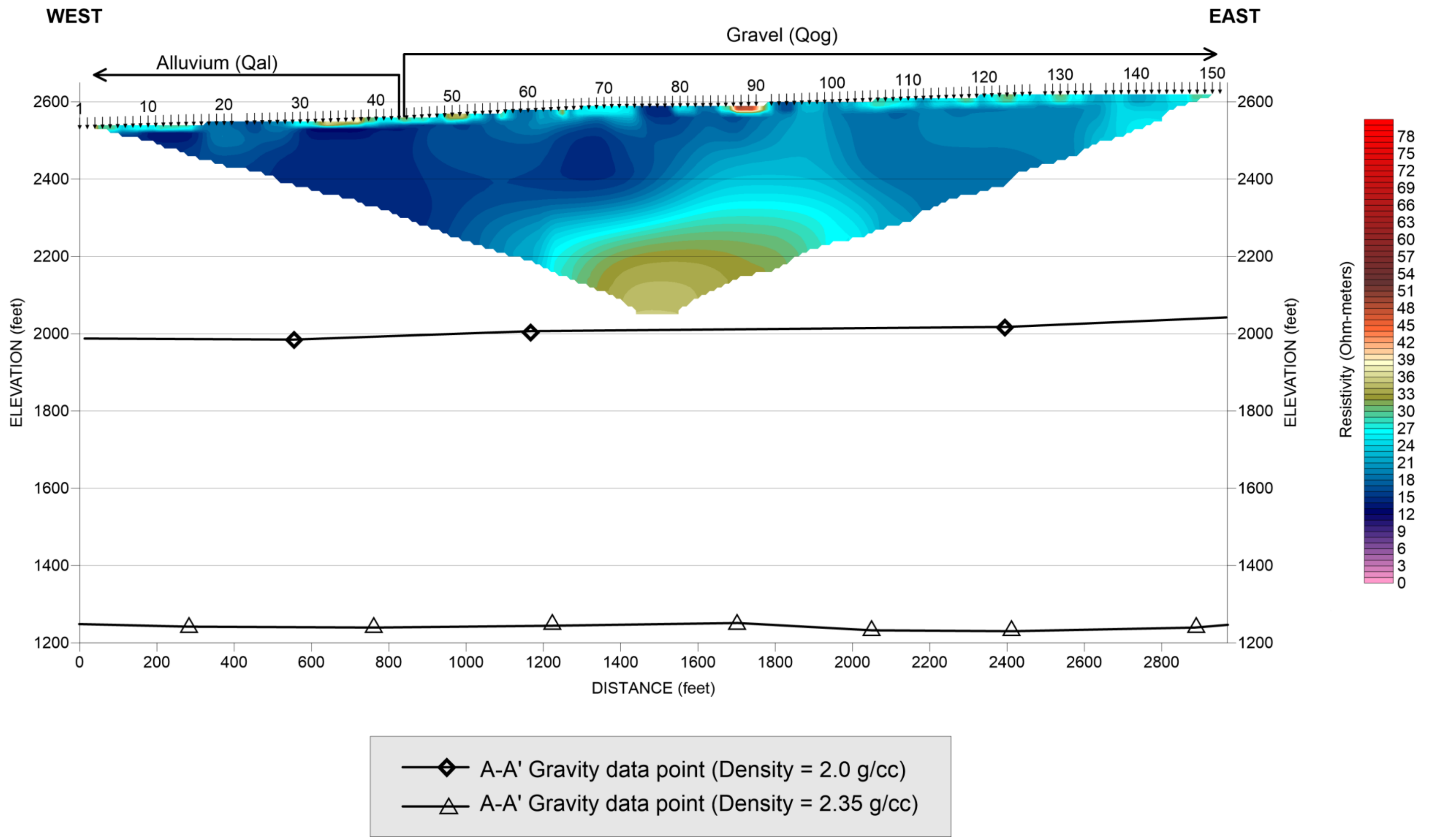

Figure 26. Combined Geophysical Results for Line 4: A) Seismic and Gravity (Density = 2.0 g/cc and 2.35 g/cc), B) Resistivity, Seismic, and Gravity (Density = 2.0 g/cc and 2.35 g/cc).

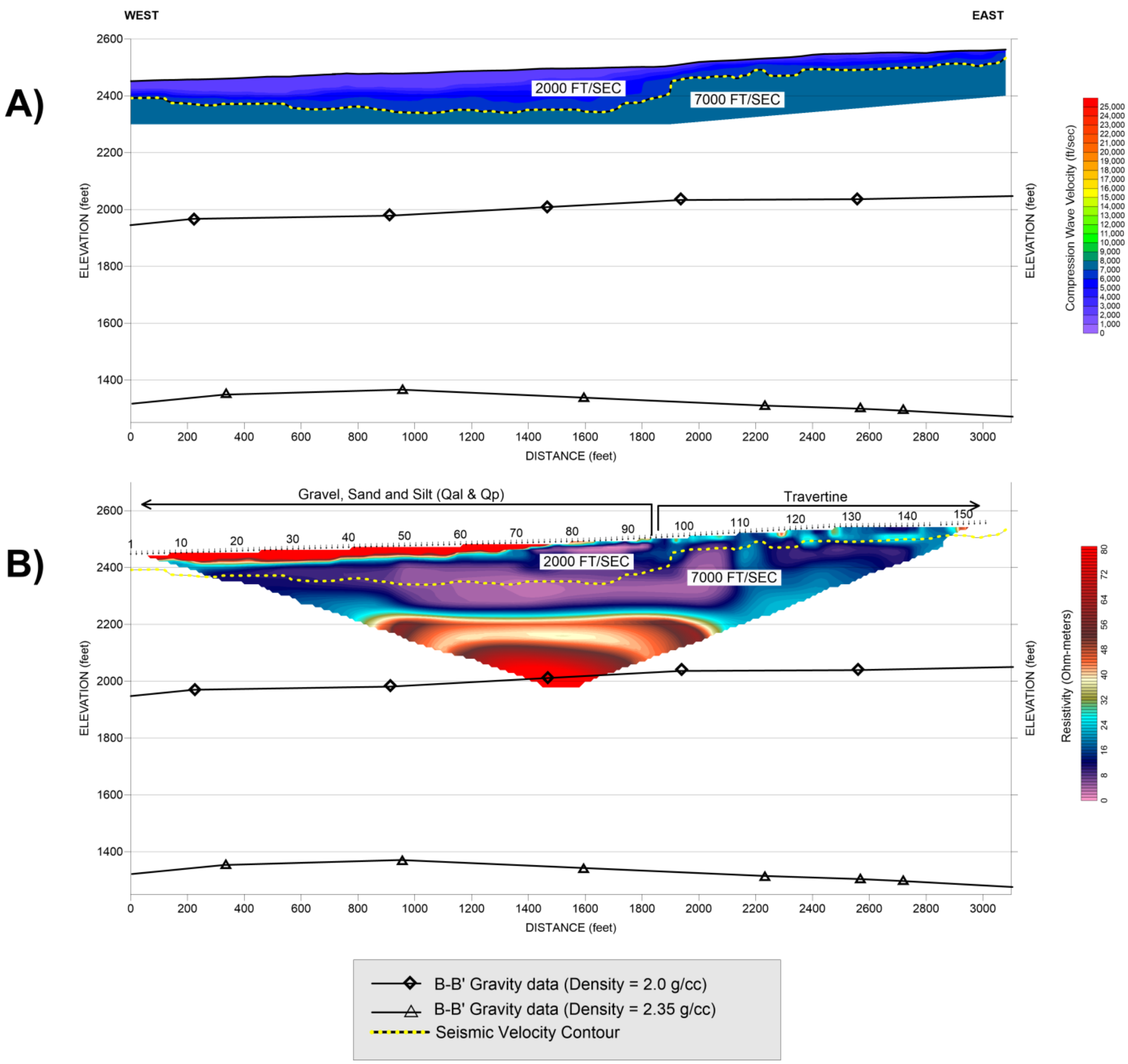

6.0 CONCLUSIONS AND RECOMMENDATIONS

A surface geophysical characterization survey was performed over a potential Tailings Storage Facility (TSF) 10 miles west of the City of Kearny, AZ in September 2017. Three electrical resistivity lines and two seismic lines were placed within the primary investigation area, as well as a broad gravity survey across the site. The objective of the characterization survey was to image depths to bedrock and evaluate changes in alluvial fill, in support of a larger program looking at the geotechnical feasibility of the proposed Peg Leg TSF.

Combined geophysical results for co-located model results were in agreement both with each other, and with geologic maps of the site. Gravel and alluvium were shown to thicken to the west of the survey site as bedrock deepened. In the region of Line 4, a travertine deposit is shown by the seismic and reisistivity data to potentially be about 50 to 60 feet thick.

Gravity measurements were acquired at 82 stations during the field investigation and additional data points were incorporated from previous investigations. In combination with the existing database, the Peg Leg site has been sufficiently mapped to provide a perspective of the basin that was otherwise unknown prior to this survey, and identify several interesting aspects of the buried bedrock surface under the proposed TSF and beyond. HGI believes that additional gravity points should be collected outside of this survey area to help understand the bigger picture. Additional points should especially include areas to the north where the CBA values and RBA values do not agree. The CBA values do not show closure and therefore indicate that the basin floor may remain deep just south of the Gila River whereas the RBA map that was created with the available data points shows a slightly different interpretation with the closure of the RBA gravity contours. Each has their own hydrological implications relative to potential placement of a TSF in this basin.

In observation of the CBA and RBA gravity, the basin is characterized by two regions defined by a gravity low, with the division roughly aligned with the location of the A-A’ model. Three gravity models were completed to help further define depths to bedrock. In past experience, HGI has made certain assumptions about density contrasts that have been subsequently confirmed by drilling campaigns. In 2010, HGI completed a gravity survey at Far West site and used two different basin fill densities to give a plausible range in depths to bedrock. Those basin fill densities of 2.0 g/cc and 2.2 g/cc were later confirmed to have underestimated the actual depth to bedrock during drilling in 2012. The density needed to create a plausible model that fit the known depth to intercepted bedrock was 2.35 g/cc. This is a much higher-than-normal basin fill density and was due in part to thick sequences of dense volcanic units encountered during drilling. To err on the side of caution for the Peg Leg site, the three models used basin fill densities of 2.0 g/cc and 2.35 g/cc to provide a range of potential depths to bedrock. If drilling is completed that intercepts bedrock, then the gravity models can be updated to reflect that depth value.

The A-A’ model characterizes an extension of shallow bedrock emanating from the western edge of the basin eastwards towards the center of the basin. This shallow buried bedrock surface is not observed elsewhere in the basin. The A-A' profile also crosses through the northern edge of the TSF footprint. Modeled depths to bedrock at the deepest portion of the basin for the two different basin fill models range from 550 ft bgs to 1250 ft bgs. The B-B' model was chosen for selection due to good road access, high density of gravity points and that it intercepts the proposed TSF footprint. Modeled depths to bedrock at the deepest portion of the basin for the two different basin fill models range from 570 ft bgs to 1300 ft bgs. The C-C' model was chosen to characterize a gravity low that occupies the northern portion of the basin and found that modeled depths to bedrock were deeper than those interpreted in the A-A' and B-B' models with depths to bedrock ranging between 700 and 1600 ft bgs. This area warrants additional gravity data collection beyond the extent of the survey to help resolve some questions that were posed in the discussion of the CBA versus the RBA gravity maps and may refine the modeled depths to bedrock.

7.0 REFERENCES

Cornwall, H.R., and Krieger, M.H. 1975, GEOLOGIC MAP OF THE GRAYBACK QUADRANGLE, PINAL COUNTY, ARIZONA: U.S. Geological Survey GQ-1206.

deGroot-Hedlin, C., and S.C. Constable, 1990, Occam's inversion to generate smooth, two-dimensional models from magnetotelluric data: Geophysics 55, 1613– 1624.

Dey, A., and H.F. Morrison, 1979, Resistivity modeling for arbitrarily shaped three-dimensional structures: Geophysics, 44, 753-780.

Ellis, R.G., and D.W. Oldenburg, 1994, Applied geophysical inversion: Geophysical Journal International, 116, 5-11.

Loke, M.H., I. Acworth, and T. Dahlin, 2003, A comparison of smooth and blocky inversion methods in 2D electrical imaging surveys: Exploration Geophysics, 34, 182-187.

Rucker, D.F., Levitt, M.T., Greenwood, W.J., 2009. Three-dimensional electrical resistivity model of a nuclear waste disposal site. Journal of Applied Geophysics 69, 150-164.

Rucker, D.F., G.E. Noonan, and W.J. Greenwood, 2011. Electrical resistivity in support of geologic mapping along the Panama Canal. Engineering Geology 117(1-2):121-133.

Sasaki, Y., 1989, Two-dimensional joint inversion of magnetotelluric and dipole-dipole resistivity data: Geophysics, 54, 254-262.

Telford, W. M., Geldart, L. P., and Sherriff, R. E., 1990, Applied Geophysics (2nd Edition), Cambridge University Press.